

Manuscript Number:	GIGA-D-17-00284
Full Title:	Arabidopsis phenotyping through Geometric Morphometrics
Article Type:	Research
Abstract:	<p>In recent years, much technical progress has been done regarding plant phenotyping including the model species <i>Arabidopsis thaliana</i>. With automated, high-throughput platforms and the development of improved algorithms for the rosette segmentation task, it is now possible to massively extract reliable shape and size parameters for genetic, physiological and environmental studies. The development of low-cost phenotyping platforms and freeware resources make it possible to widely expand phenotypic analysis tools for <i>Arabidopsis</i>. However, objective descriptors of shape parameters that could be used independently of platform and segmentation software used are still lacking and shape descriptions still rely on ad hoc or even sometimes contradictory descriptors, which could make comparisons difficult and perhaps inaccurate. Modern geometric morphometrics is a family of methods in quantitative biology proposed to be the main source of data and analytical tools in the emerging field of phenomics studies. It has been used for taxonomists and paleontologists for decades and is now a mature discipline. By combining geometry, multivariate analysis and powerful statistical techniques, it offers the possibility to reproducibly and accurately account for shape variations amongst groups. Based on the location of homologous landmarks points over photographed or scanned specimens, these tools could identify the existence and degree of shape variation and measure them in standard units. Here, it is proposed a particular scheme of landmarks placement on <i>Arabidopsis</i> rosette images to study shape variation in the case study of viral infection processes. Several freeware-based geometric morphometric tools are applied in order to exemplify the usefulness of this approach to the study of phenotypes in this model plant. These methods are concisely presented and explained. Shape differences between controls and infected plants are quantified throughout the infectious process and visualized with the appealing graphs that are a hallmark of these techniques and render complex mathematical analysis simple outcomes to interpret. Quantitative comparisons between two unrelated ssRNA+ viruses are shown and reproducibility issues are assessed. Combined with the newest automatons and plant segmentation procedures, geometric morphometric tools could boost phenotypic features extraction and processing in an objective, reproducible manner.</p>
Additional Information:	
Question	Response
Are you submitting this manuscript to a special series or article collection?	No
Experimental design and statistics	Yes
<p>Full details of the experimental design and statistical methods used should be given in the Methods section, as detailed in our Minimum Standards Reporting Checklist. Information essential to interpreting the data presented should be made available in the figure legends.</p> <p>Have you included all the information requested in your manuscript?</p>	
Resources	Yes

<p>A description of all resources used, including antibodies, cell lines, animals and software tools, with enough information to allow them to be uniquely identified, should be included in the Methods section. Authors are strongly encouraged to cite Research Resource Identifiers (RRIDs) for antibodies, model organisms and tools, where possible.</p> <p>Have you included the information requested as detailed in our Minimum Standards Reporting Checklist?</p>	
<p>Availability of data and materials</p> <p>All datasets and code on which the conclusions of the paper rely must be either included in your submission or deposited in publicly available repositories (where available and ethically appropriate), referencing such data using a unique identifier in the references and in the “Availability of Data and Materials” section of your manuscript.</p> <p>Have you have met the above requirement as detailed in our Minimum Standards Reporting Checklist?</p>	<p>Yes</p>

1 Arabidopsis phenotyping through Geometric Morphometrics

2
3 Carlos A. Manacorda¹ and Sebastian Asurmendi ^{1,2}.

4
5 ¹ Instituto de Biotecnología, CICVyA, INTA, Argentina ² CONICET, Argentina.

6 7 8 9 **Abstract**

10
11 In recent years, much technical progress has been done regarding plant phenotyping including the model
12 species *Arabidopsis thaliana*. With automated, high-throughput platforms and the development of improved
13 **algorithms for the rosette segmentation** task, it is now possible to massively extract reliable shape and size
14 parameters for genetic, physiological and environmental **studies**. The development of low-cost phenotyping
15 platforms and freeware resources make it possible to widely expand phenotypic analysis tools for
16 Arabidopsis. However, objective descriptors of shape parameters that could be used independently of
17 platform and segmentation software used are still lacking and shape descriptions still rely on *ad hoc* or even
18 sometimes contradictory descriptors, which could make comparisons difficult and perhaps inaccurate.
19 Modern geometric morphometrics is a family of methods in quantitative biology proposed to be the main
20 source of data and analytical tools in the emerging field of phenomics studies. It has been used for
21 taxonomists and paleontologists for decades and is now a mature discipline. By combining geometry,
22 multivariate analysis and powerful statistical techniques, it offers the possibility to reproducibly and
23 accurately account for shape variations amongst groups. Based on the location of **homologous** landmarks
24 points over photographed or scanned specimens, these tools could identify the existence and degree of shape
25 variation and **measure them in standard units**. Here, it is proposed a particular scheme of landmarks
26 placement on Arabidopsis rosette images to study shape variation in the case study of viral infection
27 processes. Several freeware-based geometric morphometric tools are applied in order to exemplify the
28 usefulness of this approach to the study of phenotypes in this model plant. These methods are concisely
29 presented and explained. Shape differences between controls and infected plants are quantified throughout
30 the infectious process and visualized with the appealing graphs that are a hallmark of these techniques and
31 render complex mathematical analysis simple outcomes to interpret. Quantitative comparisons between two
32 unrelated ssRNA+ viruses are shown and reproducibility issues are assessed. Combined with the newest
33 **automatons** and plant segmentation procedures, geometric morphometric tools could boost phenotypic
34 features extraction and processing in an objective, reproducible manner.

35
36
37
38
39
40
41
42
43
44
45
46
47
48
49
50
51
52
53
54
55
56
57
58 **Total word count: 11253**

59
60 **Images : 9 Tables: 2**

35
2
3
4
5
6
7
8
9
10
11
12
13
14
15
16
17
18
19
20
21
22
23
24
25
26
27
28
29
30
31
32
33
34
35
36
37
38
39
40
41
42
43
44
45
46
47
48
49
50
51
52
53
54
55
56
57
58
59
60
61
62
63
64
65

34 Introduction

35 Plant phenotyping is the process of recording quantitative and qualitative plant traits. It is key to study plant
36 responses to the environment [1].

37 A 2016 IPPN survey (https://www.plant-phenotyping.org/ippn-survey_2016) between plant scientists found
38 that most participants think that plant phenotyping will play an important role in the future, being stress
39 assessing and the model plant *Arabidopsis thaliana* mentioned between the topics of main interest.

40 Recently, many new techniques have been developed to facilitate and improve quantitative plant phenomics
41 (i.e. the full set of phenotypic features of an individual), going from destructive to non-destructive and even
42 high-throughput phenotyping [2]. Whereas the throughput is an important aspect of phenotyping, spatial and
43 temporal resolutions, as well as accuracy, should be considered [3].

44 Several workers [4–8] have developed freely available software that overcome the difficult task of rosette
45 segmentation (an issue still under investigation) by different means. This software allows several rosette
46 parameters to be computed such as area and perimeter in addition to other more complex descriptors.

47 However, the persistence of *ad hoc* descriptors [9,10] and the lack of a gold standard in this actively
48 developing field, could give rise to reproducibility issues, due to different growing substrate-segmentation
49 algorithms combinations. Moreover, different approaches give sometimes the same name to different
50 parameters (e.g. “roundness” in ImageJ [11] vs. [7]) or different names to the same parameter (e.g. “solidity”
51 in [8] equals “compactness” in [4,7] and “surface coverage” in [2]). The need of developing objective,
52 mathematically and statistically sound and more accurate shape descriptors in plants has been stressed out in
53 recent reviews on the topic [12–14].

54 Nonetheless, image datasets analyses require a conceptual and statistical corpus of knowledge that is not
55 always present in a plant biologist’s research field. Plant phenotyping relies on skills and technologies that
56 are used to characterize qualitative or quantitative traits regardless of the throughput of the analyses [1]. One
57 such knowledge corpus is morphometrics [15].

58 Traditional morphometric analyses such as measures and ratios of length, depth and width were widely used
59 in Paleontological and Zoological studies throughout the 20th century. To the end of that century the seminal
60 work of [16] was re-evaluated under the light of multivariate analysis and novel mathematical developments
61 [17,18], giving rise to modern geometric morphometrics (GM), in which was called a “revolution” in
62 morphometrics [19–21].

63 GM combines geometry, multivariate morphometrics, computer science and imaging techniques for a
64 powerful and accurate study of organismal forms. This family of methods in quantitative biology is proposed
65 to be the main source of data and analytical tools in the emerging field of phenomics [22]. Formally, GM is
66 “a collection of approaches for the multivariate statistical analysis of Cartesian coordinate data, usually (but

67 not always) limited to landmark point locations” (<http://life.bio.sunysb.edu/morph/glossary/gloss1.html>).
68 Landmark methods have been successfully applied to various species, and have the advantage of being easy
69 to understand [23].
70 Besides enhanced statistical power and better descriptive and graphical tools, GM allow researchers to
71 decompose form in size and shape, and the whole configuration of the organism under study is analyzed,
72 rather relying on the description of relative displacements of pairs of points.
73 GM is now a mature discipline that has been widely applied in biology [24–26] (see [27] for a review). In
74 plants, leaves of grapevine [28] and oak [29,30] were studied using GM methods.
75 Plant viruses cause important worldwide economic losses in crops [31]. Symptoms include plant stunting,
76 changes in leaf morphology, and sometimes plant death [32] and vary depending on various aspects
77 including genetic compatibility and environmental conditions.
78 Even given a particular host-virus interaction, different viral strains trigger different symptomatology, which
79 are more or less subtle for the observer to distinguish [33–35]. Comparing the severity of qualitative viral
80 symptoms is a difficult task performed mainly by visually rating symptoms (e.g. [36]). Consequently,
81 morphological differences could be difficult to describe and reproducibility issues could arise.
82 *Arabidopsis thaliana* (L.) Heynh. has been extensively used in studies of influences of environmental factors
83 on plants, paving the path to the development and testing of experimental techniques or data analysis
84 methods [37]. The *Arabidopsis* rosette is a nearly two-dimensional structure in the vegetative phase [8],
85 which facilitates image acquisition and interpretation.
86 Here, it is proposed a case study where GM tools are applied to study and quantitatively describe
87 morphometric changes triggered in *A. thaliana* plants by RNA viruses belonging to two unrelated families. It
88 is proposed a particular selection of landmarks to locate in the *Arabidopsis* rosette during its vegetative
89 phase. The study spans from the earlier stages of viral infection to later ones, when symptoms are already
90 visually detectable by naked eye. Comparisons are made between discriminant power of computer-assisted
91 classification and expert human eye. Symptoms severity provoked by both viruses is also compared, based
92 on the relative morphometric changes induced relative to healthy controls. Changes in allometric growth,
93 phenotypic trajectories and morphospace occupation patterns are also investigated. Size analyses are also
94 performed and the problem of growth and development modeling is discussed in the context of viral
95 infections. Throughout this work, several bioinformatics resources are applied, in order both to extract the
96 higher degree of information available, but also to exemplify different and complementary possibilities that
97 nowadays GM offers for the accurate description of shape in *Arabidopsis*.

59 Materials and Methods

Plant growth conditions

A. thaliana Col-0 seeds were stratified at 4°C for 3 days. Plants were grown under short days conditions (10 h light/14 h dark cycle, T(°C)= 23/21, Hr(%)= 60/65, and a light intensity of 150 μE m⁻² s⁻¹) in a controlled environmental chamber (Conviroon PGR14; Conviroon, Winnipeg, Manitoba, Canada). Plants were grown in individual pots in trays and treatments were assigned to plants in all trays. One experiment was performed with ORMV and two independent experiments were carried on with TuMV-UK1.

Virus infection assays

ORMV (Oilseed Rape Mosaic Virus) [38] was maintained in *Nicotiana tabacum* (cv. Xhanti nn) and infective sap was obtained after grinding infected leaves with mortar and pestle in 50 mM phosphate buffer pH=7.5. TuMV (Turnip Mosaic Virus)-UK1 strain (accession number X65978) [39] was maintained in infected *A. thaliana* Col-0. Fresh sap was obtained immediately prior to use to inoculate plants with sodium sulfite buffer (1% K₂HPO₄ + 0,1% Na₂SO₃ [wt/vol]). Mock-inoculated plants were rubbed with carborundum dust with either 50 mM phosphate buffer pH=7.5 or sodium sulfite buffer, respectively. Plants were mechanically inoculated in their third true leaf at stage 1.08 at 21 DPS, [40] because those leaves were almost fully developed by the time of the procedure and therefore constituted a source tissue for the export of virions to the rest of the plant.

Image acquisition

Zenithal photographs of individual plants growing in pots were taken with a Canon PowerShot SX50HS camera mounted in a monopod at maximal resolution. Photographs were taken at the same time of the day in successive days to minimize error. A ruler was placed in each image acquisition and only its central part (60-80 mm) was taken into account to avoid image distortion at the edges of the photograph [41].

Landmark configuration and digitization

Specimens were imaged at each DPI and .JPG files were opened with TPSUtil software, a member of the TPS Series of GM tools [42,43] that prepares the data for further analyses. Opening the output .TPS files with TPSDig2 is the first step to digitization of **landmarks**. The 11 landmarks were digitized in the same order on each picture, after setting a scale factor with a ruler, at each DPI. Eleven landmarks were recorded for each plant. Landmarks were selected to fulfill **the basic requirements for 2D** approximation [44] (see main text). Following [45] criteria, landmark 11 (which is situated at the centre of the rosette) is a **Type 1** landmark. Landmarks 1, 2, 3, 4 and 5 (which are located at the tip of leaves #8 to #12 and are the maxima of curvature of that structure) and landmarks 6, 7, 8, 9 and 10 (which are located at the intersection of the petiole and the lamina of each leaf from #8 to #12) cannot be unambiguously assigned due to the continuous nature of the leaf curvature and are Type 2 landmarks. **Each specimen was digitized in less than 1 minute.**

The Output of TPSDig2 is a .TPS file containing information about specimen name, **scale factor, and raw**

133 coordinates of each landmark for all specimens digitized. Landmark digitization was repeated to estimate
2
134 measurement error for each specimen a week after the first digitization.

135 **Validation** of the tangent space approximation

136 For a given M-dimensional structure with K landmarks (here, $M = 2$ and $K = 11$) it can be imagined an
137 individual's shape as a point in an $M \times K$ multidimensional space (a hypersphere). After centering and
138 rescaling, 3 dimensions are lost and shapes are said to be in a pre-shape space; they are not rotated yet. The
139 distance in the surface of the hypersphere at which rotation differences between shapes are minimal, is called
140 Procrustes distance. Afterwards, a reference (average) shape is selected and all other shapes are rotated to
141 minimize distances relative to it, generating a shape space and losing one more dimension (remaining $2K-4$).

142 Because distances over curved multidimensional spaces are non-Euclidean, conventional tools of statistical
143 inference cannot be used. Fortunately, for most biological shapes an approximation to Euclidean distances is
144 valid, by projecting shape points to a tangent Euclidean space (for a visual explanation see [44]). This
145 assumption should, however, be tested when new forms are being analyzed. The TPSSmall program is used
146 to determine whether the amount of variation in shape in a data set is small enough to permit statistical
147 analyses to be performed in the linear tangent space approximate to Kendall's shape space which is non-
148 linear. Since TPSSmall does not perform reflections, datasets analyzed with TPSDig2 were opened again and
149 specimens reflected when necessary to leave all clockwise rosettes.

150 Statistical analyses

151 Except otherwise stated, shape analyses were performed using MorphoJ [46] and the TPS series [42], as
152 described in the main text.

153 Student's t, Mann-Whitney, paired Hotelling's tests and rosette growth parameters analyses were executed in
154 PAST [47].

155 PTAs based on [48] were run in R [49].

156 Linear and nonlinear regressions for growth and development modeling and analysis of residuals
157 autocorrelations were performed in PAST and Infostat [50], since both software yield complementary
158 information. Lack-of-fit tests were performed in Infostat.

159 Excel 2010 was used for Durbin-Watson panel test, Holm's-Bonferroni sequential test for multiple
160 comparisons [51,52] and hyperellipses calculations using Real Statistics for Excel 2010 (ver. 4.14) [53].

163 **Results**

164 This work aims to introduce the use of GM tools for the analysis of Arabidopsis rosette phenotypes in an
165 objective and repeatable way. As such, it is not intended to offer a complete introductory explanation of each

GM tool, an objective that is beyond the scope of this paper. Such a task was already performed by [30] and for a complete introductory explanation of GM tools applied in biological systems it is recommended the lecture of [44]. Software used in this work frequently has its own user's manual and informative examples [42,46,47,50]. Nevertheless, with the purpose to facilitate the comprehension of this work to newcomers in the field of GM, each tool is briefly described prior to its application throughout the Results section.

Morphometrics aims at analyzing the variation and covariation of the size and shape of objects, defining altogether their form. Shape and form might be confusing words, used as synonyms in many languages [10]. Hereafter, it will be followed the GM definition of shape in the sense of [17] that it is "all the geometric information that remains when location, scale and rotational effects are filtered out from an object".

Landmarks digitization, Procrustes fit and outliers detection

At the heart of GM analyses is the concept of landmarks. Landmarks are discrete anatomical *loci* that can be recognized as the same point in all specimens in the study. They are homologous points both in an anatomical and mathematical sense. The selection of landmarks is based in the observance of five basic principles [44]:

- 1) Homology. Landmarks are sequentially numerated and each landmark must correspond to the same number of landmark in all specimens under study.
- 2) Adequate Coverage of the Form. Landmarks should be chosen in a way they cover up the maximum possible extent of the form of interest. It is important to bear in mind that a region not included between landmarks is not analyzed.
- 3) Repeatability. The same landmarks should be easily identified in the same structure in order to avoid measurement error.
- 4) Consistency of Relative Position. This attribute guarantees that landmarks do not interchange relative positions.
- 5) Coplanarity. For 2D-landmarks, an assumption of coplanarity is required to avoid measurement error.

There is no absolute landmark configuration on any given structure. The choice of the number of landmarks and their configuration depend on the hypotheses being tested. Here, the focus of the analyses is on the phenotypic impact of viral infections on the Arabidopsis rosette through time. Hence, short-day conditions were chosen to delay flowering, allowing the plant's aerial part to remain near two-dimensional during the experiment. To encompass as broadly as possible the phenotypic changes experienced by the plant during the infection, chosen landmarks should not only be present from earlier stages to the infection to later ones, but also be placed in regions that experience dramatic changes upon infection. A relatively reduced number of landmarks can be used to describe complex forms [30,54].

An 11-landmark configuration for the Arabidopsis rosette is shown in Figure 1A (see Materials and Methods). Plants were inoculated in their third true leaf (24 plants were mock-inoculated and 17 were

ORMV-infected) and images were acquired starting from three **days post-inoculation (DPI)** to 12 DPI (see Materials and Methods). Leaves below number 8 were not chosen for landmark placement for three main reasons: a) they are hidden for younger leaves at later stages of infection b) these old leaves had almost finished their growth by the time the first photographs were taken (and the form covered would be a less informative one for the process of shape and size change upon viral infection) and c) the senescence process of older leaves lead to morphological changes derived from dehydration and death. Younger leaves (beyond leaf number 12) were not chosen because they were not present at the earlier stages of infections, therefore violating the requisite of repeatability of **landmarks.**

A flowchart of data analyses throughout this paper is shown in Figure 1B. Image datasets for all DPIs and both treatments **were handled and digitized for further analyses using the TPSUtil and TPSDig2 software** generating .TPS **output files. Digitization process was performed twice (see Materials and Methods).**

Several freeware could be used to extract shape information from .TPS files [44]. Here, the MorphoJ software [46] was chosen mainly because of its ease to use and comprehensive tools available. MorphoJ creates new datasets from several file extensions, including .TPS. The “Supplementary file ORMV.morphoj” was created and 16 datasets were generated, one for each DPI and digitization instance. Specimens were classified according with ID, Treatment, DPI and Digitization for each dataset. Combinations of classifiers were also done to perform further grouped analyses.

The first step of shape analysis in GM consists in extracting shape coordinates from raw data obtained at the digitization step. The procedure that has become standard in GM studies is the Generalized Procrustes Analysis (GPA).

The purpose of Procrustes procedures is to remove from the specimens all information that is not relevant for shape comparisons, including size. Specimens are firstly translated at the origin (“superimposed”) by subtracting the coordinates of its centroid from the corresponding (X or Y) coordinates of each landmark. Then, differences in size are removed rescaling each specimen to the mean centroid size (CS) (CS is calculated as the square root of the summed squared distances of each landmark from the centroid, ~~giving a linearized measure of size~~). Differences in rotation are eliminated by rotating specimens minimizing the summed squared distances between homologous landmarks (over all landmarks) between the **forms**. ~~The process starts with the first specimen, and then an average shape is found that now serves as a reference. It proceeds iteratively over all specimens until no further minimization of average distances are found [55].~~

MorphoJ performs a full Procrustes fit, which is a variant of the analysis that is more conservative and resistant to outliers of shape.

In Arabidopsis, the arrangement of organs along the stem (phyllotaxy) follows a predictable pattern, the Fibonacci series. Phyllotaxy orientation can be either clockwise or counter-clockwise [56]. This should be

233 taken into account because clockwise and counter-clockwise rosettes are biological enantiomorphs like right
2 and
234 and left hands and must not be superimposed by GPA. Opportunely, MorphoJ automatically performs
4
235 reflections on every specimen when executing a GPA and therefore it is not a problem at this stage, but care
6
236 must be taken when using different software.

237 After executing a full Procrustes fit of each dataset, they were inspected for the presence of outliers. The
8
238 shape of one Mock-inoculated plant (M2) diverted the most from the rest in 11 out of 16 datasets. Therefore,
11
239 it was excluded from all datasets for successive analyses.

240 Afterwards, datasets were combined and the “Combined dataset 3-12 DPI” was created with 640
13
241 observations included following a common GPA. Then, a wireframe was created that connects consecutive
15
242 landmarks. This tool aids visualization, as will be explained later. Next, the “Combined dataset 3-12 DPI”
17
243 was subdivided by DPI. This creates one dataset for each DPI, each one with the two digitization outputs for
20
244 each plant.

245 **Validation of the tangent (Euclidean) space approximation**

246 **Prior to conducting** further analyses, a basic assumption of GPA-based GM analysis should be tested: that the
24
246 projections of shapes in Kendall’s shape space onto a tangent Euclidean shape space are good
26
247 approximations for the studied shapes. This task is performed by basically comparing the Procrustes
28
248 distances (the conventional measure of a morphometric distance in geometric morphometrics [57]) obtained
31
249 using both shape spaces (see Materials and Methods). Two subsets of data were created for each DPI, one
33
250 with Mock-inoculated and the other with ORMV-infected plants. **Next, datasets were manually combined**
35
251 using a text editor to create three main datasets (Mock, ORMV and ALL plants). TPSSmall (v.1.33) was then
37
252 used to compare statistics for distance to reference shape both in Tangent (Euclidean) and Procrustes
39
253 (Kendall’s) shape space for both treatments separately and for all plants together (Supplementary Table 1).
40

254 **Results showed that maximum Procrustes distances from mean (reference) shape were 0.371 (ORMV), 0.405**
42
255 **(Mock) and 0.400 (ALL). They are all well below the largest possible Procrustes distance ($\pi/2 = 1.571$).**
44
256 **Mean Procrustes distances from mean (reference) shape were 0.168 (ORMV), 0.186 (Mock) and 0.184**
46
257 **(ALL). This indicates a closer arrangement of ORMV shapes in shape space relative to Mock-inoculated**
48
258 **plants. Tangent and Procrustes distances were very similar (Supplementary Table 1) and regressions through**
49
259 **the origin for distance in tangent space, Y, regressed onto Procrustes distance, X, showed slopes > 0.98 and**
50
260 **correlations > 0.9999 for all groups (Supplementary Table 1 and Supplementary Figure 1). This results are in**
51
261 **line with several similar analysis performed onto a variety of biological forms [30,58–60].**
53
262

263 **Testing measurement error and variation between treatments using Procrustes ANOVA**

264 As mentioned before, two digitizations were performed on each plant at each DPI, in order to evaluate
57
265 measurement error. This procedure is important because digitization error should always account for far less
59
266

266 variance in the subsequent analyses than specimens and treatments do [30]. There are the differences
267 between specimens and particularly between treatments that are worth investigating, not human error in
268 landmark placement. Purposely, datasets for each DPI were combined and subjected to a hierarchical
269 analysis of variance (ANOVA). In MorphoJ this is a Procrustes ANOVA, with “Treatment” as an additional
270 main effect, “ID” for the individuals and “Digitization” as the Error1 source. In Procrustes ANOVA,
271 variance is partitioned by means of hierarchical sum of squares (SS) which implies that each effect is
272 adjusted for effects that appear earlier in the hierarchy. This is taking into account the nested structure of the
273 data (an issue that is crucial if the design is unbalanced, i.e., with unequal sample sizes as is here the case),
274 thus allowing one to quantify differences in Treatments and plants regardless of Treatment. The variance
275 unexplained by any of these effects is measurement error and it is estimated using the differences between
276 digitizations. Hence, total variance was decomposed into main (treatment) and random (ID and digitization)
277 components and was expressed as a percentage of total variance for each DPI. The analysis is executed
278 simultaneously for both size and shape. Results are shown in Supplementary Table 2. Explained variance (as
279 a % SS) for which ~~measurement~~ error accounted for was in the range of 0.01 and 0.12 for size and 0.40 and
280 1.15 for shape over all DPIs. Thus, measurement error was negligible throughout the digitization process.
281 Detailed analysis of results shown in Supplementary Table 2 revealed that for size, the Individual (ID) effect
282 was highly significant at each DPI as evidenced by Goodall’s F-test ($p < 0.0001$). Treatment effect was
283 insignificant from 3 to 5 DPI but starting from 6 DPI the virus affected the plant’s size ($0.0001 < p < 0.03$).
284 For shape, the Individual effect was also highly significant at each DPI as evidenced both by Goodall’s F-test
285 ($p < 0.0001$) and by MANOVA (standing for Multivariate Analysis of Variance) results ($p < 0.0001$).
286 Treatment impacted earlier shape than size, since as soon as 5 DPI differences in shape were detected ($p <$
287 0.001).

288 **Ordination Methods and shape change visualization**

289 **PCA**

290 Once shape variables (the 22 Procrustes Coordinates) are extracted for all specimens at each DPI, it is useful
291 to plot differences between individuals and treatments. However, patterns of variation and covariation
292 between lots of variables are difficult to envision particularly because ~~geometric~~
293 **biologically** nor statistically independent [44]. PCA is a technique that allows simplifying those patterns and
294 making them easier to interpret. By performing a PCA, **shape variables are replaced with complex variables**
295 **(principal components, PCs) that do not covary but carry all the information.** Moreover, as PC axis are
296 orthogonal and independent, and most of the variation in the sample usually can be described with only a few
297 PCs, shape analysis could be restricted to very few axes, avoiding the need of jointly interpret dozens of
298 variables. It is important to keep in mind that PCA is useful for the comparison between individuals, not

299 groups, and though a powerful descriptive tool, it does not involve any statistical test. Therefore, the relative
300 separation of groups in a PCA plot does not allow one to extract conclusions about significant differences (or
301 its absence).

302 Firstly, this technique was used to inspection error measurement (previously quantified by Procrustes
303 ANOVA, Supplementary Table 2). A covariance matrix was created for the “Combined dataset 3-12 DPI”
304 and then a PCA was performed. Scatterplots were generated for the first 4 PCs, which together account for
305 87.2 % of the total variance (Figure 2). The proximity of equally colored points indicates a small digitization
306 error.

307 As measurement error explained a negligible percentage of variance, digitizations were averaged within
308 specimens and DPIs. From the “Combined dataset 3-12 DPI” it was created the “Combined dataset 3-12 DPI,
309 averaged by ID DPI” dataset, which contains all the 320 averaged observations. The averaged data were used
310 to find the directions of maximal variance between individuals. A covariance matrix was generated and a
311 PCA performed. PC1 accounted for 64.2 % of total variance and the first 4 PCs summed up to 87.4 % of it.
312 PCs 4 and beyond accounted for less than 5 % of variation each and are therefore of little biological interest.

313 Afterwards, PCA output was used for which is one of its main purposes in GM: visualization of shape
314 change. Three types of graphs were obtained: PC shape changes (a diagram showing the shape changes
315 associated with the PCs); Eigenvalues (a histogram showing the percentages of total variance for which the
316 PCs account) and PC scores (a scatterplot of PC scores).

317 PC Scatterplots show the distribution of specimens along the axes of maximum variance (Figure 3A, B). To
318 aid visualization, dots corresponding to early stages (3-6 DPI) were lightly colored and later ones (7-12 DPI)
319 were darker colored. Results evidenced that PC1 is a development-related axis, because clearly separated
320 early (mostly negative values) from late (positive values) stages of the experiment (Figure 3A). Moreover, at
321 later stages ORMV-infected plants scored less positive in this axis, suggesting that infected plants retained a
322 more juvenile (pedomorphic) shape. Positive extremes of PC2-4 are related to ORMV shapes.

323 To this point, GM visualization tools are used to better understand what these relative positions on
324 scatterplots mean respect to shape differences.

325 *Visualization of shape changes*

326 Prior to showing graphs from the “PC shape changes” tab, a brief description of common GM visualization
327 tools is needed in order to accurately interpret the results. After the GPA, every configuration in the sample
328 is optimally aligned to the average configuration and nearly optimally aligned to every other configuration in
329 the sample. GPA removed differences attributable to size, position and orientation from configurations. All
330 differences that remain are shape variation. Accordingly, shape differences are found using the relative
331 displacements of the landmarks from one shape to another shape nearby in shape space [61]. By

332 superimposing a target shape to a starting shape and looking for the relative displacement of homologous
2
333 landmarks from one shape to another, insights on how variation between shapes occurs can be obtained and
4
334 hypotheses about the underlying mechanisms, proposed.
6

335 A key concept to bear in mind is that it is fundamentally wrong to consider landmarks displacements in an
9
336 isolated manner [44,61]. This is because all the landmarks included in the GPA jointly determine the
10
337 alignment of each configuration in relation to the mean shape. Then, variation in the position of each
11
338 landmark after superimposition is relative to the positions of all other landmarks. Though a shift is shown at
12
339 every landmark, these shifts are relative to all other landmarks. Lollipop and wireframe graphs are based on
13
340 these assumptions (see below).
14
16
18
19

341 Shape variation could be depicted by means of transformation grids. Transformation grids are
21
342 mathematically constructed following the thin-plate spline technique, whose detailed explanation is far from
22
343 the objective of this work and has been explained elsewhere (Klingenberg, 2013; Zelditch et al., 2012).
23
344 Briefly, landmarks of a starting shape are placed on a grid of an imaginary infinitely thin metal plate.
24
345 Landmarks of a target configuration are placed on another grid of equal characteristics, and both metal sheets
25
346 are superimposed. Each landmark in the starting shape (e.g., mean shape) is linked to its homologous to
26
347 reach the target configuration, and the deformation caused in the spline is calculated finding the smoothest
27
348 interpolating function that estimates energy changes in the spline between landmarks. Importantly,
28
349 differently from lollipop or wireframe graphs, transformation grids distribute the change in landmark
29
350 positions to the space between landmarks, where no objective information is available. Then, whereas a
30
351 powerful descriptive tool, transformation grids must be carefully interpreted, especially regarding regions of
31
352 the object that do not have landmarks nearby positioned (Klingenberg, 2013; Zelditch et al., 2012,). More
32
353 details and examples are given below.
33
34
35

354 Wireframe graphs (Figure 3C-F) connect the landmarks with straight lines for the starting and target shapes,
355 thus showing the relative displacements of landmarks from a mean shape. Negative values of PC1 mostly
356 correspond to juvenile (and infected) shapes; positive values of PC1 belong to healthy controls and adults.
357 Hence, by depicting the -PC1 component, target shapes have negative values (Figure 3C). It can be seen that
358 -PC1 explains the relative shortening of leaves #11 (landmarks 4 and 9) and #12 (landmarks 5 and 10). It
359 makes sense, since younger plants have yet to develop these relatively new leaves. Petioles of leaves #10,
360 #11 and #12 are particularly shortened. Relative to these shortenings, older leaves (#8 and #9) are relatively
361 longer but, interestingly, only its laminae, since its petioles are not relatively elongated. Taken together, PC1
362 reveals that ORMV impaired the elongation of newer leaves to their normal extent. PC2 (Figure 3D)
363
364
365

363 associates with relative radial displacements of leaves; tips of leaves #8 and #9 (landmarks 1 and 2) come
364 close together, lowering the typical angle between successive leaves from near 137.5° to close to 90° . These
365 relative displacements determine that leaves #9 and #10 form an exaggerated angle of near 180° . PC3 (Figure
366 3E) also mostly relates to radial changes in the infected rosette: leaf #10 is relatively displaced towards leaf
367 #8 and the main effect is, again, the increase of the angle between leaves #9 and #10 to near 180° . PC4
368 (Figure 3F) explains less proportion of total variance (4.5%) and its effect is less clear; it is mostly related to
369 the relative displacement of the lamina of leaf #11 towards leaf #9, almost without altering its petiole, which
370 functions as a hinge. Leaves #9 and #10 are, as a combination of the effects depicted by PC2 and PC3, both
371 relatively displaced towards leaf #8. Taken together, the wireframe visualization of the first four PCs (which
372 account for more than 87% of total variance) show that ORMV induces the relative shortening of laminae
373 and (especially) petioles of newest leaves, which relates to a pedomorphic shape, and provokes the relative
374 displacement of leaves #9 and #10 towards leaf #8.

375 Displacement vectors (called “lollipop graphs” in MorphoJ) are arrows drawn between a landmark in a
376 starting shape and the same landmark in a target shape. The dot in the lollipop represents the starting position
377 and the vector is represented by a line departing from it (but in some software the inverse convention is
378 followed, i. e., PAST). Though these visualization are being displaced in the GM literature in favor of more
379 advanced tools [61], here it is presented the case for -PC1, showing the relative displacements of landmarks
380 (Figure 3G). It can be directly compared with Figure 3C.

381 Lastly, transformation grids are exemplified for -PC1 in Figure 3H-I. Figure 3H depicts the starting (mean)
382 shape. Figure 3I show the transformed grid for -PC1. The compression of the grid in the central zone is the
383 result of the relative displacement of landmarks 3, 8 (leaf #10), 4, 9 (leaf #11) and 5, 10 (leaf #12) towards
384 the center of the rosette, whereas grid stretching is detected around landmarks 1 and 2 (revealing the relative
385 expansion of laminae of leaves #8 and #9, since its petioles remain relatively immobile, landmarks 6 and 7).
386 As stated above, visualization with these grids should be cautiously interpreted since the interpolation
387 function deforms the grid between places where no landmarks are placed (and no information about even the
388 existence of tissue is guaranteed). Therefore, only regions near landmarks should be discussed when viewing
389 these graphs. To see these changes in more detail, PCA analyses were performed for each DPI. The
390 “Combined dataset 3-12 DPI, averaged by ID DPI” was subdivided by DPI performing a common Procrustes
391 fit, creating eight new datasets (DPIs) (raw data in Supplementary file ORMV.morphoJ) . Covariance
392 matrices were generated and a PCA performed for each DPI dataset. PC1 accounted for between 27-43 % of
393 total variance and the first 4 PCs summed up from 78 to 84 % of it. PCs beyond PC4 accounted for 5 % or
394 less of variation each. Shape change visualization showed that PC1 gradually separated specimens belonging

395 to different treatments. Mock-inoculated plants were progressively more aligned with positive PC1 values.
396 PC2 was more generally related to ORMV-infected plants in its positive values. Relative shortening of
397 younger leaves and petioles, and relative displacement of leaves towards leaf #8 were progressively more
398 accentuated (Supplementary Figure 2).

399 **Discriminant Analysis**

400 So far, differences between individuals were addressed with the aid of PCA. Afterwards a Discriminant
401 Analysis (DA) was performed to test whether differences between treatments exist.

402 DA is a technique mathematically related to PCA. It finds the axes that optimize between-group differences
403 relative to within group variation. It can be used as a diagnostic tool [44]. It is here used for testing
404 treatments using a series of tests for sample mean differences including an estimate of the accuracy of shape
405 in predicting groups. The capability of DA to correctly assign specimens to treatments was assessed along
406 the experiment using the averaged datasets for each DPI. In MorphoJ, Discriminant Function Analysis was
407 requested selecting “Treatment” as classification criterion. By default, DA in MorphoJ performs a parametric
408 Hotelling’s T-square test, and here there were also requested permutations tests for the Procrustes and
409 Mahalanobis distances with 1000 random runs. Hotelling’s test is the multivariate equivalent of the common
410 Student’s t-test. Procrustes and Mahalanobis distances show how far shapes from one group are from the
411 mean of the other group. Results of the tests are shown in Table 1. At 5 DPI the three tests found shape
412 differences between treatments ($0.001 < p < 0.005$). From 6 DPI and beyond, p-values were extremely
413 significant ($p < 0.0001$). These results coincide with those obtained by Procrustes ANOVA of shape
414 (Supplementary Table 2). DA maximizes group separation for plotting their differences and predicting group
415 affiliation (classification). The classification of a given specimen (through the discriminant axis) is done
416 using functions that were calculated on samples that included that same specimen (resubstituting rate of
417 assignment). Then, a degree of over-fitting is unavoidable and leads to an overestimate of the effectiveness
418 of the DA. To overcome this problem, one solution is to use a cross-validation or jackknife procedure
419 [30,44]. Jackknife procedure leaves one specimen at a time not used for constructing the Discriminant
420 function and then tests the rate of correct specimen assignment. Only jackknife cross-validated classification
421 tables provide reliable information on groups. Results of DA in group assignment are shown in Figure 4 for
422 3, 7 and 12 DPI and detailed for all DPIs in Supplementary Table 3. As expected, resubstitution rates of
423 assignment (Figure 4A, D, G) were higher than jackknifed counterparts (Figure 4B, E, H), but the latter
424 reached high levels of accuracy ($\geq 90\%$) from 6 DPI and beyond (Supplementary Table 3). To test whether
425 this level of accuracy was indeed good, these results were compared with classification/misclassification
426 tables completed by human observers. The entire image dataset of 7 DPI was given to three expert
427 researchers working with Arabidopsis (one of the authors (S. Asurmendi) and two other researchers from

another Institution). They were all blind to the assignment of treatments to each plant, except for one Mock-inoculated and one ORMV-infected plant that were given as references. They classified the 38 remnant plants and results are shown in Supplementary Table 3. Human accuracy ranged from 55 to 72.5 %, with an average of 64.2 %. Therefore, DA outperformed expert human eye by 30 % at 7 DPI and yielded higher classification rates from 5 DPI.

Wireframe graphs for 3, 7 and 12 DPI (Figure 4C, F, I) show the difference from Mock group to ORMV group. There is little difference at 3 DPI, if any (Figure 4C), consistently with nonsignificant differences found by DA at this stage. At 7 DPI (Figure 4F), the relative shortening of leaf #11 (landmarks 4 and 9) is evident, as is the relative increase in the angle between leaves #9 and #10. These tendencies persisted at 12 DPI (Figure 4I). At this stage, petioles of leaves #11 and #12 are strongly relatively shortened. These results resemble those obtained in Figure 3C-F and approximately summarize shape changes explained by the first 4 PCs, indicating that these shape differences not only separated juveniles from adults but are also hallmarks of shape change induced by ORMV. These results are interesting because discriminant axes not necessarily resemble PCA axes [44].

Allometric patterns and size correction

As ORMV induced not only changes in shape, but also in size (Supplementary Table 2) it is worth investigating whether shape changes are associated to size differences. In principle, group differences could arise if individuals of one group are different in shape because they grew faster than the other group's individuals and reached earlier a more advanced developmental stage. The association between a size variable and the corresponding shape variables is called allometry. Isometry, by contrast, is the condition where size and shape are independent of each other and usually serves as the hypothesis null. These concepts are rooted in the Gould-Mosimann school of allometry that conceptually separates size and shape [62]. Though size had been removed from forms after GPA, leaving shape differences free of it, there could be a linear relationship between them. Allometry can be statistically tested for by tests of multiple correlation. When groups are present, a single regression line through all groups cannot be fit to test allometry because lines could have group-specific slopes or intercepts [30]. As TPSRegr (see below) uses raw data coordinates and averaged by ID DPI datasets in MorphoJ do not have them, these analyses were carried on with individual datasets from only the 1st Digitization. As proven earlier, differences between digitizations were negligible (Figure 2 and Supplementary Table 2).

To test whether an allometric component is present in each group, separate regressions were performed for each treatment and DPI with Procrustes Coordinates as dependent variables and ln(CS) as the independent variable. Permutation tests were requested with 10.000 runs. Respective p-values and predicted SS from regressions (which correspond to allometric variation of shape) are shown in Figure 5A. Allometry

461 accounted for moderate to high proportions of the total shape variation since SS reached values of 36% at 6
2
462 **DPI (Mock)**. ORMV induced a reduction in the allometric component of shape variation as evidenced by
4
463 lower predicted SSs along the experiment and non-significant values of allometry for all except 4 and 5
6
464 DPIs. For both treatments and particularly for healthy controls, a bell-shaped curve is detected and a
8
465 maximum of allometry is seen at 6 DPI for Mock plants but a day before for ORMV. Differences between
10
466 treatments start sharply at 5 DPI, when allometry accounts for 32% of predicted SS for Mock but only 20%
11
467 for ORMV. This analysis shows that for ORMV, shape variation is much less driven by size heterogeneity
13
468 (at a given DPI) and that for Mock plants this situation (isometry) occurs at later stages of development (10-
15
469 12 DPI).

17
470 **When at least one group has regression slopes different from zero a series of tests could be done in order to**
18
471 **control for size and repeat analyses to assess whether differences in shape are actually the result of size**
19
472 **variation only [29,30,44,62]. TPSRegr (v. 1.41) was used firstly to determine whether group-specific slopes**
20
473 **were parallel at each DPI (3-8). Only at 3 and 4 DPI this occurred ($p > 0.05$, slopes not statistically**
21
474 **significant). As slopes were found to be parallel, it is possible to test whether they are separate parallel slopes**
22
475 **or coincident (same Y-intercept). TPSRegr tests demonstrated that slopes are coincident ($p > 0.05$). Then,**
23
476 **size-corrections could only be done for 3 and 4 DPI, since from 5 to 8 DPI slopes were different ($p < 0.05$)**
24
477 **and groups follow its own allometric pattern and for 10 and 12 DPI there are isometry and size do not**
25
478 **correlate with shape variation. Size-correction was done for 3 and 4 DPI separately in MorphoJ, using all 40**
26
479 **plants. Shape variables were regressed onto $\ln(\text{CS})$ for each dataset, pooling regressions within subgroups**
27
480 **(treatments) and permutation tests with 10.000 runs were requested. Residuals from the analyses contain the**
28
481 **size-free information about shape only and can be used to repeat DAs to test for improved accuracy of**
29
482 **discrimination [62]. Results (Figure 5B-E) showed that group separation was not improved. This is**
30
483 **somewhat expected since at this stage of viral infection there are no detectable differences in size nor shape**
31
484 **yet (Figure 4 and Tables 1-3). This test and the large overlap between populations in the scatterplot of**
32
485 **regression scores onto size (Figure 5F, G) suggest that the effect of size on shape is very similar for both**
33
486 **treatments and DPIs: bigger rosettes have further distal displacements of leaves #10, 11 and 12 relative to**
34
487 **older leaves (#8 and #9) and elongated petioles (Figure 5H, I) thus reflecting the differential internal growth**
35
488 **of the rosette. Bigger, more mature rosettes have more developed newest leaves.**

489 **Phenotypic Trajectory Analyses (PTA)**

490 Whilst the comparison of allometric vectors indicated that shape change is altered at definite DPIs during
51
491 ORMV infection, a holistic view of ontogenetic alterations needs to measure phenotypic evolution across
52
492 multiple levels. It allows ontogenetic patterns to be characterized as phenotypic trajectories through the
53
493 morphospace, rather than phenotypic vectors. The method proposed by [48] “(...) *may also be used for*
54
55
56
57
58
59
60
61
62
63
64
65

494 determining how allometric or ontogenetic growth trajectories differ, or for quantifying patterns in other
495 data that form a time-sequence” [48]. Briefly, phenotypic trajectories have three attributes: size, direction
496 and shape.

497 Trajectory size (MD) quantifies the path length of the phenotypic trajectory expressed by a particular group
498 across levels. This represents the magnitude of phenotypic change displayed by that group. If trajectories of
499 two or more groups compared over comparable time periods differ in trajectory size then it indicates
500 differences in rates of morphological change.

501 Trajectory direction (θ) is a multivariate angle that describes the general orientation of phenotypic evolution
502 in the multivariate trait space. Statistical comparisons of trajectory direction can be used to provide an
503 assessment of patterns of convergence, divergence, and parallelism.

504 Trajectory shape (D_{Shape}) describes the shape of the path of phenotypic evolution through the multivariate
505 trait space. This information is useful because it indicates whether there are differences in how each group
506 occupies the morphospace through the time period.

507 **PTA** analysis proceeds by starting from the PCs for all specimens at all DPIs. They were obtained from the
508 “Combined dataset 3-12 DPI, averaged by ID DPI” of the Supplementary file ORMV.morphoj. **The R script**
509 **developed by [48] was run in RStudio [49].**

510 PTA approach (with 1,000 residual randomization permutations) revealed significant differences in the
511 magnitude of phenotypic evolution between the two treatments ($MD_{Mock,ORMV} = 0.100$, $P_{size} = 0.003$),
512 implying that ORMV-infected plants experienced a lower rate of ontogenetic phenotypic evolution relative to
513 controls. Overall direction of ontogenetic changes were also statistically significantly different ($\theta_{Mock,ORMV} =$
514 18.34° , $P_\theta = 0.001$). Finally, shape assessment analysis showed differences between treatments regarding
515 trajectories over time ($D_{Shape_{Mock,ORMV}} = 0.367$, $P_{Shape} = 0.001$) (Table 2). When phenotypic trajectories are
516 plotted through time for the first two principal components (Figure 6) these statistical conclusions are
517 graphically confirmed. Group trajectories diverge from 3 DPI and trajectory lengths are evidently different,
518 specifically regarding the relative stasis of the ORMV-infected group beyond 6 DPI. Both factors contribute
519 to the overall difference found in trajectory shape.

520 However, as pointed out by [63], no one method of disparity measurement is sufficient for all purposes.
521 Using a combination of techniques should allow a clearer picture of disparity to emerge. With this aim,
522 another available approach to compare shape trajectories through multivariate morphospace was used.
523 Originally developed to study unequal morphological diversification in a clade of South American fishes
524 [64], this approach is useful because allows investigating whether a group “explores” different amount of
525 morphospace than others, additionally to possible differences in magnitude of phenotypic evolution.

Moreover, density parameters (D) could be calculated to determine whether the amount of morphological change is more or less constrained in the morphospace.

The method was adapted to the present case study: as there is not a phylomorphospace and both treatments lack a “common ancestor” but each plant follow its own independent ontogenetic path, nodes and branches do not exist. Rather, each plant possesses its own trajectory without points in common. Taken these considerations into account, morphological trajectories were calculated for all plants. To do so, the “Combined dataset 3-12 DPI, averaged by ID DPI” of the Supplementary file ORMV.morphoj was subdivided by ID. Forty new datasets (Mock- and ORMV-inoculated plants from the same previously performed Procrustes fit) were obtained and Procrustes Coordinates and eigenvalues from the 7 PCs obtained were exported to an Excel spreadsheet.

The morphometric change experienced by a plant throughout ontogeny equals the Euclidean distance (D) between successive points in morphospace that represent its shape at each DPI. As PCs from a PCA carry all the morphological information extracted from the Procrustes Coordinates, distances are simultaneously calculated over all the PCs using the Pythagorean Theorem. These distances are designated as morphometric path lengths ($\Sigma D = MPL$) (sensu [64]). Mock-inoculated plants traveled on average more distance through morphospace than infected ones ($MPL_{Mock} = 0.6956$ vs. $MPL_{ORMV} = 0.5963$, $p = 0.00025$, Mann-Whitney test). Other measures are traditionally used to detect changes in morphospace occupation patterns and the amount of difference between character states among specimens in morphospace [63], e.g. sum of variances (ΣVar). Control plants had higher ΣVar values than infected plants ($\Sigma Var_{Mock} = 0.0350$ vs. $\Sigma Var_{ORMV} = 0.0230$, $p = 2.52 \times 10^{-6}$, Mann-Whitney test) a result that pointed to a higher increase in shape change in controls [63]. Morphospace density occupation measures could be obtained taking into accounts not only MPLs but also variances of the PCs across the experiment. If a group folded an equivalent amount of morphometric change into a much smaller region of morphospace than the other, thus will have a higher density [64]. Morphometric path density (D) could be calculated as $D_1 = MPL/\Sigma Var$. ORMV-infected plants are more densely restricted in morphospace ($D_{1(Mock)} = 20.21$ vs. $D_{1(ORMV)} = 26.93$, $p = 2.89 \times 10^{-6}$, Mann-Whitney test) (Table 2).

An alternative measure of density ($D_2 = MPL/V$) considers the volume (V) that the group occupies in morphospace. A variety of volumetric measures are possible [63]. This study considered the volume of a 95% confidence hyperellipse. It was obtained by calculating the square root of the product of the eigenvalues of the PCs and comparing them with expected values for a X^2 distribution at $\alpha = 0.05$ (see Materials and Methods). Mock-inoculated plants have hyperellipses of higher volume on average than infected plants ($Hyperellipse_{(IC95\%)}_{Mock} = 0.0129$ vs. $Hyperellipse_{(IC95\%)}_{ORMV} = 0.0073$), but differences were not statistically significant ($p = 0.11888$, Mann-Whitney test). Similarly, density measures based on hyperellipses

calculations were not statistically significantly different ($D_{2(\text{Mock})} = 111.47$ vs. $D_{2(\text{ORMV})} = 146.34$, $p = 0.25051$, Mann-Whitney test), although ORMV-infected plants had a higher average density. These differences in density measures could arise from the fact that hypervolume calculations can produce values that are extremely small and variable. Since the hypervolume is calculated by taking the product of univariate variances, any axis or axes with negligible variance will produce a value of hypervolume close to zero. Moreover, all multiplied variances are given the same weight and consequently, PC axes that represent a minimal percentage of the total variance could distort conclusions obtained with more informative axes. Thus, hypervolume can be very sensitive to variation in a single character. To avoid this issue, only the axes with significant variances are chosen to represent the disparity among points in morphospace [63]. Therefore, the analysis was repeated including only the first three PCs, which accounted for more than 95% of variance. Results were similar to previously obtained for all parameters but hyperellipse's volumes were found to be statistically significantly different (Hyperellipse_{(IC95%)Mock} = 0.022 vs. Hyperellipse_{(IC95%)ORMV} = 0.014, $p = 0.0052597$, Mann-Whitney test) as the D_2 parameter ($D_{2(\text{Mock})} = 32.97$ vs. $D_{2(\text{ORMV})} = 41.87$, $p = 0.040172$, Mann-Whitney test) (Table 2).

Taken together, PTA showed that Mock-inoculated and ORMV-infected plants follow separate paths through morphospace. They differ in length, direction and shape (Figure 6), but also explore distinct regions of morphospace in a disparate quantity. Control plants experience more diversification of shape, as evidenced by the comparative length of trajectories (MD and MPL), have a higher amount of difference between shape states through the experiment in morphospace ($\sum\text{Var}$) and explore more ample regions of morphospace (D_1 , D_2) (Table 2). On the whole, ORMV infection not only alters the direction of ontogenetic shape development but also diminishes shape change.

Growth and Development modeling

Even after finding that Mock- and ORMV-infected plants follow different ontogenetic trajectories of shape it is possible to compare their rates and timings of growth and development. When groups have different ontogenetic trajectories of shape, it is necessary to use a formalism that can be used when treatments follow group-specific ontogenetic trajectories [44]. One such possibility is to compare the rates and timings at which groups depart from their own juvenile forms [65], an approach that can be applied to compare growth [66] and development [67] rates between groups with different ontogenetic trajectories. To linearize the relationship between size and age, $\ln(\text{CS})$ was regressed on $\ln(\text{DPI})$ and growth rates were compared. Results showed higher growth rate for Mock (1.06, $\text{CI}_{95\%}=1.00-1.12$) than for ORMV (0.72 $\text{CI}_{95\%}=0.64-0.79$) ($p_{(\text{same slope})}= 3,0309\text{E}-12$) (Figure 7A). Lack-of-fit was assessed for both regressions and rejected ($p= 0.9975$ and $p= 0.3144$ respectively), thus indicating the goodness of fit for both linear regressions. To compare developmental rates, it was measured the rate at which shape progressively

592 differentiates away from that of the youngest age class (3 DPI) from 4 to 12 DPI. The degree of
593 differentiation is measured by the morphometric distance between each individual and the average of the
594 youngest age class [67], using Euclidean distances as approximations of Procrustes distances (Supplementary
595 Figure 1 and Supplementary Table 1). Linear regressions with Euclidean distances (D) as a dependent
596 variable and $\ln(\text{DPI})$ as a regressor indicated a higher developmental rate for Mock- (0.34, $\text{CI}_{95\%}=0.32-0.36$)
597 relative to ORMV-infected plants (0.24, $\text{CI}_{95\%}=0.22-0.26$) ($p_{(\text{same slope})}= 5,4657\text{E}-13$) (Figure 7B). Lack-of-fit
598 was rejected ($p= 0.1626$ and $p= 0.3278$ respectively). Healthy controls depart more from its own juvenile
599 shape from 8 DPI and beyond (Figure 7C), indicating that developmental change was relatively impaired by
600 ORMV. Together, these results indicated that ORMV reduced both growth and morphological change.

601 **Alternatively, nonlinear models have been widely applied to studies of growth in several biological**
602 **species (reviewed in [44]), including Arabidopsis [6]. The latter decided to apply a logistic model regarding**
603 Arabidopsis growth from seedling stage on the basis of the prevalence of that model in plant growth studies.
604 However for the present study it was decided to follow a less aprioristic approach, more in line with that of
605 [67] who tested several nonlinear models and compared their relative performance regarding absence of
606 residuals autocorrelation, percentage of variance explained and minimal parameterization. Here, five
607 nonlinear models were chosen to compare: Logistic, Gompertz, Exponential, Monomolecular and Richards
608 [67]. For development analysis (Euclidean distances respect to 3 DPI mean shape) Logistic model fitted the
609 best, with minimal Mean Square Error and low correlation between parameters, very close to the Gompertz
610 model. However, all tested models showed a strong autocorrelation of residuals as evidenced for the Durbin-
611 Watson panel test (Appendix S1). When the residuals are autocorrelated, it means that the current value is
612 dependent of the previous (historic) values and that there is a definite unexplained pattern in the Y variable
613 (Euclidean distance in this case study) that shows up in the disturbances. As a basic assumption of these
614 analyses is the independence of residuals and particularly, their absence of autocorrelation, neither analyzed
615 model fitted the development accurately. The same problem was found when the five growth models were
616 applied to study growth, regardless choosing CS or $\ln(\text{CS})$ as the dependent variable and DPI or $\ln(\text{DPI})$ as
617 the regressor (data not shown). An explanation for the autocorrelations of residuals is that data from
618 successive DPIs (intra-group analyses) are not independent: every specimen is recorded at each DPI. This
619 leads to a multivariate longitudinal data analysis situation, a branch of statistical analysis that has been
620 recently addressed following different approaches [68], and whose level of complexity is beyond the scope
621 of this work.

622 However, intra-treatment paired comparisons of shape are possible using a paired Hotelling's test (a
623 multivariate analog of the paired t-test). It was found a strong effect of time on shape and differences are
624 extremely statistically significant for Mock plants (Supplementary Table 4).

625 Basic rosette growth and development parameters were studied (Figure 7). Rosette Growth,
2 Absolute Growth Rate (AGR) and Relative Growth Rate (RGR) had been proposed as measures of rosette
626 expansion and its velocity and rate, respectively [2,4]. Mock-inoculated plants were statistically significantly
4 bigger from 6 DPI and beyond (Figure 7D). The graphic lacks the typical sigmoidal shape of growth curves,
627 probably because early stages of development (when landmarks used in this work were not present yet) were
628 not included in the analysis and plant growth had not reached its plateau phase at 12 DPI yet. AGR and RGR
8 analyses revealed an early change in growth tendencies between treatments. As early as between 3 and 4
629 DPI, (two days before the detection of significant differences in rosette area) ORMV started to slow rosette
10 growth relative to healthy controls (Figure 7E-F). AGR graphic (Figure 7E) shows that, in contrast with
11 control plants, ORMV-infected plants grew less rapidly from one day to the following throughout the
13 experiment with the exception of the period between 8 and 10 DPI. This indicated different growth
15 acceleration for each treatment. Growth acceleration (Figure 7G) peaked between 5 and 6 DPI in control
630 plants and remained near zero until 12 DPI, suggesting a stage of linear rate of expansion. Later on, negative
22 acceleration could indicate an entering in plateau phase reached by the region of the rosettes under study. In
631 infected plants, however, acceleration between 5 and 6 DPI was negative and differed strongly from controls
24 (difference = 1.94 mm²/day², p= 0.0009, Mann-Whitney test), indicating that ORMV early slowed down the
632 velocity of plant growth in a drastic manner. A trend towards more negative values of growth acceleration
26 relative to controls was maintained in ORMV-infected plants until 10 DPI, though only marginally
633 statistically significant. At 10-12 DPI both groups decelerate their growth, possibly indicating an entering in
28 a plateau phase of growth. These results indicate that ORMV induces measurable changes in growth rates
634 before the mean CS is found to be statistically significantly different from healthy controls, and that the
30 acceleration of growth, which is characteristic from several growth models, is impaired by the virus.
31

41 A similar approach was followed to investigate developmental differences between groups. Mean
42 developmental rates were calculated between consecutive DPIs (Figure 7H). Mock –inoculated plants
643 showed a higher mean developmental rate from 5 DPI to the end of the experiment. The Mean
44 Developmental Acceleration (Figure 7I) showed a more complex pattern: Mock-inoculated plants peaked at
645 5 DPI and after that, a deceleration of development was detected until 12 DPI. In infected plants, though,
46 acceleration reached a maximum at 6 DPI and then sharply decreased towards more negative values than
646 control plants, indicating a relative stagnation in morphological change. At 12 DPI ORMV induced a less
48 negative value of Mean Acceleration of development than controls, although its velocity remained lower
647 ((Figure 7H-I).
50

57 Taken together, these results show that ORMV impacts both growth and development very early after
648 infection. Whereas a direct measure (CS) detected differences between treatments at 6 DPI, more elaborated
59

parameters (AGR, RGR and Mean Developmental Acceleration) allowed differences to be detected as soon as 4 DPI. Growth and developmental patterns differed between treatments in a dissimilar manner: AGR showed differences in growth velocities at 4 DPI, whilst Mean Developmental Rate was clearly different later on. Acceleration graphics (Figure 7G,I) indicated that ORMV has an early effect in decelerating both growth and development, but the latter was more dramatically affected in comparison with relative growth deceleration whose decrease was more or less stepwise. Mock-inoculated plants peaked developmental acceleration at 5 DPI and growth acceleration the following day. ORMV-infected plants peaked developmental acceleration at 6 DPI but lost the subsequent growth acceleration phase (Figure 7G,I). This and other comparisons indicate that ORMV does not just induce delayed growth or morphological change patterns, but a more radical change in the coordination of both parameters.

Comparison with TuMV infections

As stated earlier, one goal of applying the GM approach to the study of Arabidopsis is to make phenotypic comparisons in a more objective and repeatable manner. To this end, the same experimental setup was applied to the study of viral infections of *A. thaliana* with TuMV, an ssRNA+ virus unrelated to ORMV (<http://viralzone.expasy.org/>). The experiment spanned from 4 to 10 DPI since at 12 DPI excessive curling of some leaves induced by TuMV impaired the correct assignment of landmarks (Supplementary file TuMV 1st.morphoj). Individual datasets were created for each DPI and Procrustes Coordinates extracted. A combined dataset was created and PCA carried on. After outliers exclusion, 27 Mock and 14 TuMV-inoculated plants remained. PCA revealed that PC1 accounted for 49.2% of total variance (much less than the ORMV experiment accounted for) and PC1 plus PC2 accounted for 69.3% of total variance. Again, PC1 mostly separates juveniles from adult rosettes and negative values related predominantly to infected plants which retained a more immature phenotype (Figure 8A). It was supported by the associated wireframe graph which depicts a relative shortening of leaves #11 and #12, similarly to ORMV-infected plants (Figure 3C). PC2 was strongly positively related to infected plants and, similarly to the ORMV case (Figure 3D), reflects the widening of the angle between leaves #9 and #10. PCs 3 and 4 (Figure 8B-C) accounted for 17.7% of total variance and are mainly negatively related to TuMV infection. Discriminant Analysis (Figure 8D-E) showed that, similarly as observed with ORMV, group means were statistically significantly different starting from 5 DPI. Wireframe graphs also evidenced a strong relative shortening of the petioles, similarly to that had been found under ORMV infections (Figure 4F,I), indicating that more compact rosettes are a common outcome of these viral infections. Discriminant power was slightly higher for almost all DPIs in the case of TuMV (Supplementary Table 5, Supplementary Table 3). Moreover, Procrustes Distances were higher for every DPI in the case of TuMV, which induced a Procrustes separation at 8 DPI only matched at 12 DPI for ORMV-infected plants (Supplementary Table 5, Table 1). These results suggest that TuMV is a

691 more severe virus than ORMV is in Arabidopsis, since it induces a more pronounced departure from Mock
692 mean shape.
693 PTA supported this evidence: A subset of 4-10 DPI datasets were selected to compare ORMV with TuMV
694 infections (Table 2, Figure 9A-B). Whilst trajectory size difference ($MD_{Mock, TuMV}$) was similar to the obtained
695 with ORMV, the multivariate angle ($\theta_{Mock, TuMV}$) that separates infected from healthy trajectories more than
696 doubled that of ORMV. Shape differences ($D_{ShapeMock, TuMV}$) between trajectories almost doubled. The
697 majority of the other measures indicated a slower rate of shape change relative to Mock plants, similarly to
698 ORMV infection, but relatively less marked (Table 2). To visualize and compare shape changes,
699 transformation grids with Jacobian expansion factors and lollipops were done in PAST for 10 DPI plants
700 (Figure 9C-D). Both viruses induced relative contraction of the rosette around leaf #11 (the most affected),
701 but TuMV induced more severe deformations. To confirm these results and to test for the reproducibility of
702 the analysis, an independent experiment of TuMV infection was executed (Supplementary file TuMV
703 2nd.morphoj). PTA analyses were run and trajectory attributes compared (Table 2). There were obtained
704 very similar results relative to the first TuMV experiment.
705 Together, these results indicated that both TuMV and ORMV induced relative developmental arrest as well
706 as shape change, but symptoms triggered by ORMV are mainly driven by developmental arrest whereas
707 TuMV also promotes shape change in a relatively higher extent, thus impacting more strongly on overall
708 shape.

710 Discussion

711 Here, several standard GM tools were applied to the study and comparison of morphological changes
712 induced in Arabidopsis by viral infections. GM analysis is a powerful approach due both to its statistical
713 toolbox and its appealing visual analysis of shape change. By conceptually separating size and shape, making
714 them mathematically orthogonal, both factors that determine form could be separately analyzed. Thus, the
715 effect of ORMV infection was detected earlier on shape and the derived measures of size (Tables 1-3, Figure
716 7E,F) than in size itself (Figure 7D). GM analysis greatly outperformed diagnosis when compared against
717 expert human eye (Supplementary Table 3). The effect of time on shape was more pronounced than that of
718 treatment, since the former was detected earlier (Tables 2 and 5). This was particularly the case for control
719 rosettes, reflecting that normal rosette development is not a scaling up of previous shapes but a relative
720 displacement of newly developed structures, a process that is somewhat impaired by ORMV, which induced
721 the retention of a more juvenile-like phenotype (Figure 3).

722 Normal allometric growth comprised a lengthening of petioles and laminae of new leaves (#11 and 12)
723 relative to older ones (Figure 5H-I). This process was reversed by ORMV, which also distorted the normal

2
725
4
726
6
727
8
728
11
729
13
730
15
731
17
732
19
733
20
734

angle of approximately 137.5° between successive leaves. As a result, leaves #9 and 10 bended towards leaves #8 and 11, which in turn came close together, bending towards the inoculated leaf (#3) that is situated middle way between them (Figure 4F,I). TuMV provoked similar outcomes (Figure 8) but the effect seemed stronger, not only regarding the distorted inter-leaves angle, but for the relative contraction of leaf #11 respect to all remaining leaves, including #12 (Figure 8E, Figure 9C-D). Taking into account the source-to-sink nature of viral movement by phloem [34] and its radial structure [69] it could be hypothesized that virus or viral-induced hormones are distributed through the rosette in such a way that they inhibit proximal systemic growth. **These kind of data-based hypothesis is one desired outcome of the application of GM tools [44] in particular and phenotyping in general.** Future work should test this hypothesis by means of comparing cell number or size in distal and proximal parts of systemic leaves, or the effect growth hormones and mutants have in these parameters.

22
735
24
736
26
737
28
738
29
739

Both viruses diminished shape change, constraining virus-infected rosettes to smaller regions of multivariate morphospace (Supplementary Table 1, Table 2 and Figures 6-9). **Ontogeny (the development or course of development of an individual organism) is a genetically-based endogenous process but can be altered by the environment [65].** Here, the departure of normal ontogenetic development is induced by both viruses. The consequences of this departure should be analyzed by further work measuring relevant traits.

31
740
33
741
35
742
37
743
39
744
40
745
42
746
44
747
46
748
48
749
50
750

The availability of a **standard measurement unit of shape change (Procrustes distance)** allowed to compare ORMV- and TuMV- induced shape changes relative to the departure from healthy control shapes (Figure 9A-B, Tables 2-4 and 6) and objectively rank symptoms severity. Besides, visualization tools aided to identify were the shape change differences allocated in the rosette (Figure 4C, F, I, Figure 8D-E and Figure 9C-D). In sum, it was concluded that TuMV impacts more strongly on Arabidopsis rosette shape than ORMV does. Trajectory and density parameters could be also used to compare developmental phenotypic plasticity (a term generally used to summarize how a given group responds to a series of different environmental conditions by producing an array of phenotypes [70]). Multivariate reaction norms could be then obtained, using shape variables but also controlling for other variables (size, external factors) and weighting their interaction. This would enrich the description of phenotypes whilst offering a solid basis for comparisons.

51
751
52
752
53
753
54
754
55
755
56
756
57
757
58
758
59
759
61
62
63
64
65

As superior organisms, plants have complex shapes that experience complex changes throughout their life spans, particularly when exposed to severe stresses that modify the route of ongoing development. Regarding so, their complex phenotypes are difficult to encompass in all their extent by using only one technique, regardless of its descriptive or statistical power. This note is of importance when evaluating the capabilities and limitations of the GM tools presented here. For example, whereas we showed that ORMV significantly impacts rosette shape from 5 DPI and beyond (Supplementary Table 2 and Table 1), and learnt from the wireframes (Fig. 4C, F, I) that some laminae and (mostly) petioles become relatively shorter under ORMV infection, no particular statistical statement could be done about these discrete phenotypic outcomes. Rather, if these questions were to be specifically addressed, other measures (such as direct measures of petioles´

length) should have been taken. GM analyses performed here pointed to overall shape (and size) changes, and visualization tools could serve as guides to further study the putative underlying mechanisms involved if required. Also, as pointed out above, landmarks analyses come with the limitation of not being capable of extrapolate results to the regions between them without uncertainty. Because of that, the selection of a specific set of landmarks (covering the region of interest) must be well stated at the beginning of the experiment and be sound to study the problem of interest. As with any other technique, caution is needed when interpreting the results in order to consider its limitations.

After the genomic revolution, there is a need of objective, reproducible, and accurate assessments of morphology as a critical missing link to supporting phenomics [71]. The use of GM allows standardizing deviations from controls in a consistent, objective manner. At the core of these conceptual framework is the GPA, which permits to compare shapes in Procrustes units of distance.

The examples given in this work are necessarily limited, but other applications could be easily envisioned: as the choice of landmarks placement is arbitrary on a given structure, other experimental setups could place them differently to study different stages of growth or other anatomical regions of interest. Importantly, this technique is not a competitor but a possible complementation of newly developed automated platforms for rosette segmentation. It is now possible for some platforms to identify the tip of leaves, the center of the rosette and the intersection between lamina and petiole [6,72], thus giving the landmarks used in this study and its coordinates, automatically.

Moreover, the same software used in this work permits GM 3D image analysis, therefore allowing the study of plant species with a more complex architecture.

100 years after the revolutionary vision of D´Arcy Thompson´s transformation grids and more than 40 years since the beginning of the revolution in morphometrics, GM application for plant phenotyping is starting to develop [29,30,73] and the plant model species *Arabidopsis thaliana* should benefit from it.

ACKNOWLEDGEMENTS

We thanks Dr Flora Sánchez and Dr Fernando Ponz for the kind gift of ORMV and TuMV virus. We thank Dr. Ken Kobayashi and Nicolás Carlotto for human treatment assignments of plants in the Discriminant Analysis comparison, Dra. Valeria Carreira for critical reading of the manuscript and Mariano Manacorda for assistance in adapting figure colours to the Color Universal Design for accessibility to colour-blind people. This research was supported by PICT 2014-1163 from Agencia Nacional de Promoción Científica y Tecnológica (ANPCyT) and by project PE 1131022 (INTA). The authors declare that they have no conflict of interests.

Figures and Tables Legends

794 **Figure 1. (A)** Landmark configuration in an Arabidopsis rosette. An 8 DPI Mock-inoculated rosette is
795 shown. (B) Analysis flowchart showing the different software used in this study, with main features extracted
796 from each one listed below corresponding icon. See main text and Materials and Methods for details.

797 **Figure 2.** Shape variation including all observations and replicas. PCA scatterplots of (A) PC1 vs. PC2 and
798 (B) PC3 vs. PC4. Equally colored dots represent both digitizations of the same specimen, for all DPIs. The
799 **scale factor for this graph is directly the magnitude of the shape change as a Procrustes distance;** the default
800 **is 0.1, which corresponds to a change of the PC score by 0.1 units in the positive direction.**

801 **Figure 3.** Shape variation between specimens (averaged by measurement replicates). PCA scatterplots of (A)
802 PC1 vs. PC2 and (B) PC3 vs. PC4, which together explain 87.4 % of variance. Pale dots = juvenile (3-6 DPI)
803 plants. Dark dots = mature (7-12 DPI) plants. (C-F) Wireframe graphs showing shape changes from the
804 starting (average) shape (bluish green) to the target shape (orange) for the first four PCs. Negative (PC1) and
805 positive (PCs2-4) components are shown, respectively. Here and throughout this work, leaf number is
806 indicated in the wireframe in black. (G) Lollipop graph for the -PC1 component. Lollipops indicate starting
807 position of landmarks with dots. (H-I) Transformation grids for (H) the starting shape and for (I) the target
808 shape (-PC1). Shape changes (C-G and I) are magnified 2X for better visualization.

809 **Figure 4.** Discriminant analyses of shape variation between treatments at 3 (A- C), 7 (D-F) and 12 (G-I) DPI.
810 Frequencies of discriminant scores obtained by resubstitution rates of assignments (A, D, G) and a jackknife
811 cross-validation (B, E, H) are shown using histogram bars with percentages of correct assignments above
812 each graph. Wireframes comparing mean shapes (C, F, I) are shown magnified 2 times. Mock = bluish green;
813 ORMV = orange.

814 **Figure 5.** Allometric analyses. (A) Predicted sum of squares from regressions of shape onto $\ln(\text{CS})$ for each
815 treatment and DPI. P-values were corrected using Holm's sequential test ($\alpha=0.05$). * = $p < 0.05$; ** = $p <$
816 0.01 . Allometric analyses for (B, D, F, H) 3 DPI and (C, E, G, I) 4 DPI (Mock = bluish green; ORMV =
817 orange). Cross-validated DAs before (B-C) and after (D-E) size correction with percentages of correct
818 assignments above each graph. (F-G) Scatterplot of regression scores vs. $\ln(\text{CS})$. (H-I) Wireframes showing
819 starting mean shape (turquoise) and target shape depicting an increase in one unit of $\ln(\text{CS})$ (blue), without
820 magnification.

821 **Figure 6.** Phenotypic trajectories for Mock and ORMV (3-12 DPI). Scatterplot shows the first two PCs of
822 shape variation across the experiment. Mean values for each DPI are colored and connected with lines. PTA
823 parameters are given (see main text). Mock = bluish green; ORMV = orange.

824 **Figure 7.** Growth and Development modeling. Comparisons of (A) growth and (B) developmental rates.
825 Linear regressions for Mock (black lines) and ORMV (orange) with CI95% bands (blue). (C) Euclidean
826 distances from own average juvenile shapes for mock and ORMV plants. Student's t tests were performed

827 separately for each DPI, contrasting mock vs. ORMV mean distances from its own average shapes at 3 DPI.
828 Bars indicate mean average shape distances from average juvenile shape +/- SE. ** = $p < 0.01$; *** = $p <$
829 0.0001. (D-G) Rosette growth parameters. Measures of (D) size, (E-F) growth rate and (G) growth
830 acceleration. Error bars indicate +/- SE. * = $p < 0.05$; ** = $p < 0.01$; *** = $p < 0.0001$, Mann-Whitney tests.
831 (H-I) Rosette developmental parameters. (H) rate and (I) acceleration. (C-I) Mock = bluish green; ORMV =
832 orange.

833 **Figure 8.** Summary of GM analyses for TuMV-infected plants. (A-C) Shape variation between specimens.
834 (A) PCA scatterplot (PC1 vs. PC2). Pale dots = juvenile (4-5 DPI) plants. Dark dots = mature (7-10 DPI)
835 plants. Wireframe graphs from starting (average) shape (bluish green) to target shape (reddish purple)
836 corresponding to -PC1 (to the left) and +PC2 (top) are included. (B-C) Wireframes for -PC3 and -PC4,
837 respectively. (D-E) Frequencies of jackknifed discriminant scores for 7 and 10 DPI respectively, with
838 wireframes depicting shape changes included. Wireframes show starting shape (mock = bluish green) to the
839 target shape (TuMV = reddish purple). Shape change is magnified 2X.

840 **Figure 9.** Comparison of virus severity. PC plots of PTA for (A) ORMV- and (B) TuMV-infected plants,
841 compared with Mock-inoculated plants (4-10 DPI). PTA parameters are shown (see main text).
842 Transformation grids with lollipops and Jacobian expansion factors were executed in PAST for (C) ORMV-
843 and (D) TuMV-infected plants depicting shape change from controls at 10 DPI. Jacobian expansion factors
844 indicate expansions of the grid (yellow to orange red for factors > 1) or contractions (blue for factors
845 between 0 and 1). Lollipops indicate target position of landmarks with dots. Leaf #11 (landmarks 4 and 9) is
846 positioned at the bottom.

847 **Table 1.** Statistical tests for differences between means of treatments at each DPI from DA. Permutation
848 tests with 1000 random runs.

849 **Table 2.** Comparative trajectory analyses for the full dataset of the ORMV experiment (3-12 DPI), the
850 reduced dataset (4-10 DPI) and the comparisons with TuMV experiments (4-10 DPI).

851 Appendix S1. Description of the Durbin-Watson panel test.

852 Supplementary Figure 1. Graphical assessment of the Tangent shape space approximation. Scatterplots of
853 distances in the tangent space against Procrustes distances (geodesic distances in radians) for (A) Mock-
854 inoculated plants, (B) ORMV-infected plants and (C) all plants, over all DPIs. A blue line is plotted to show
855 a slope of 1 through the origin. Then a least-squares regression line through the origin is shown in red (for
856 data in which the variation in shape is small this will hide the blue line).

857 Supplementary Figure 2. Wireframes depicting shape change associated with -PC1 values from 3 to 12 DPI
858 (A-H). Green = starting (average) shape; red = target shape. No magnification was applied.

860 Supplementary Table 1. Summary statistics for the comparisons between Tangent (Euclidean) and Procrustes
2 shape distances from average shapes and for regression slopes and correlations between the two distances.
861
4
862 Supplementary Table 2. Summary of centroid size and shape variation. Hierarchical sum of squares
6
863 ANOVA. Main effect: Treatments; random factors: Individuals (ID), Digitization. SS, MS and df refer
8
864 respectively to sum of squares, mean sum of squares (i.e., SS divided by df) and degrees of freedom. Error1
9
10
865 = Measurement error.
11
12
866 Supplementary Table 3. Classification/misclassification tables from DA for each DPI and human observers
13
867 for 7 DPI.
14
15
868 Supplementary Table 4. Statistical comparisons of intra-treatment shape changes across the ORMV
16
869 experiment. Holm's-Bonferroni sequential correction at $\alpha=0.05$.
17
18
870 Supplementary Table 5. Discriminant Analysis for TuMV. Statistical tests for differences between means of
19
20
871 treatments at each DPI from DA (with permutation tests with 1000 random runs) and
21
22
872 classification/misclassification tables for each DPI.
23
24
873
25
26
874
27
28
29
30
31
32
33
34
35
36
37
38
39
40
41
42
43
44
45
46
47
48
49
50
51
52
53
54
55
56
57
58
59
60
61
62
63
64
65

875
2
3
876
5
877
7
878
9
879
11
880
13
881
15
882
17
883
19
884
21
885
23
886
25
887
27
888
29
889
31
890
32
891
34
892
36
893
38
894
40
895
42
896
44
897
46
898
48
899
50
900
51
901
53
902
55
903
57
904
59
60
61
62
63
64
65

Bibliography:

1. Granier C, Vile D. Phenotyping and beyond: modelling the relationships between traits. *Current Opinion in Plant Biology* [Internet]. Elsevier Ltd; 2014;18:96–102. Available from: <http://linkinghub.elsevier.com/retrieve/pii/S1369526614000259>
2. Vanhaeren H, Gonzalez N, Inzé D. A Journey Through a Leaf: Phenomics Analysis of Leaf Growth in *Arabidopsis thaliana*. *The Arabidopsis Book* [Internet]. 2015;13:e0181. Available from: <http://www.bioone.org/doi/10.1199/tab.0181>
3. Dhondt S, Wuyts N, Inzé D. Cell to whole-plant phenotyping: the best is yet to come. *Trends in Plant Science* [Internet]. 2013 [cited 2017 Apr 27];18:428–39. Available from: <http://www.sciencedirect.com/science/article/pii/S1360138513000812>
4. De Vylder J, Vandenbussche F, Hu Y, Philips W, Van Der Straeten D. Rosette tracker: an open source image analysis tool for automatic quantification of genotype effects. *Plant physiology* [Internet]. 2012 [cited 2014 Mar 25];160:1149–59. Available from: <http://www.pubmedcentral.nih.gov/articlerender.fcgi?artid=3490612&tool=pmcentrez&rendertype=abstract>
5. Green JM, Appel H, Rehrig EM, Harnsomburana J, Chang J-F, Balint-Kurti P, et al. PhenoPhyte: a flexible affordable method to quantify 2D phenotypes from imagery. *Plant methods* [Internet]. 2012;8:45. Available from: <http://www.pubmedcentral.nih.gov/articlerender.fcgi?artid=3546069&tool=pmcentrez&rendertype=abstract>
6. Tessmer OL, Jiao Y, Cruz J a, Kramer DM, Chen J. Functional approach to high-throughput plant growth analysis. *BMC systems biology* [Internet]. BioMed Central Ltd; 2013 [cited 2014 Mar 25];7 Suppl 6:S17. Available from: <http://www.ncbi.nlm.nih.gov/pubmed/24565437>
7. Camargo A, Papadopoulou D, Spyropoulou Z, Vlachonasios K, Doonan JH, Gay AP. Objective definition of rosette shape variation using a combined computer vision and data mining approach. *PLoS ONE*. 2014;9.
8. Ispiryanyan R, Grigoriev I, Castell W, Schäffner AR. A segmentation procedure using colour features applied to images of *Arabidopsis thaliana*. *Functional Plant Biology*. 2013;40:1065–75.
9. Krieger JD. Controlling for Curvature in the Quantification of Leaf Form. In: Elewa AMT, editor. *Morphometrics for Nonmorphometricians*. Springer Berlin Heidelberg; 2010. p. 27–71.
10. Bonhomme V, Picq S, Gaucherel C, Claude J. Momocs: outline analysis using R. *Journal of Statistical Software* [Internet]. 2013;56:1–24. Available from: <http://www.jstatsoft.org/v56/i13/paper%5Cnpapers3://publication/uuid/9FA27917-592B-4216-85D5->

905 BA4A85B8E698
2

906 11. Schneider CA, Rasband WS, Eliceiri KW. NIH Image to ImageJ: 25 years of image analysis. Nat Meth
3
4
907 [Internet]. Nature Publishing Group, a division of Macmillan Publishers Limited. All Rights Reserved.;
5
6
908 2012;9:671–5. Available from: <http://dx.doi.org/10.1038/nmeth.2089>
7
8

909 12. Lobet G. Image Analysis in Plant Sciences: Publish Then Perish. Trends in Plant Science [Internet]. 2017
9
10
910 [cited 2017 Jul 12];22:559–66. Available from:
11
12
911 <http://linkinghub.elsevier.com/retrieve/pii/S1360138517300912>
13
14

915 13. Bucksch A, Atta-Boateng A, Azihou AF, Battogtokh D, Baumgartner A, Binder BM, et al.
15
16
916 Morphological Plant Modeling: Unleashing Geometric and Topological Potential within the Plant Sciences.
17
18
917 Frontiers in Plant Science [Internet]. 2017 [cited 2017 Jul 12];8:900. Available from:
19
20
918 <http://www.ncbi.nlm.nih.gov/pubmed/28659934>
21
22

919 14. Balduzzi M, Binder BM, Bucksch A, Chang C, Hong L, Iyer-Pascuzzi AS, et al. Reshaping Plant
23
24
916 Biology: Qualitative and Quantitative Descriptors for Plant Morphology. Frontiers in Plant Science
25
26
917 [Internet]. Frontiers; 2017 [cited 2017 Jul 12];8:117. Available from:
27
28
918 <http://journal.frontiersin.org/article/10.3389/fpls.2017.00117/full>
29
30

920 15. Strauss RE. Foreword. In: Elewa AMT, editor. Morphometrics for Nonmorphometricians. Springer
31
32
921 Berlin Heidelberg; 2010. p. v–vi.
33
34

922 16. Thompson DW. On Growth and Form. Dover; 1917.
35
36

923 17. Kendall DG. The diffusion of shape. Advances in Applied Probability [Internet]. 1977 [cited 2017 Apr
37
38
924 27];9:428–30. Available from:
39
40
925 https://www.cambridge.org/core/product/identifier/S0001867800028743/type/journal_article
41
42

926 18. Kendall DG, Kendall WS. Alignments in two-dimensional random sets of points. Advances in Applied
43
44
927 Probability [Internet]. 1980 [cited 2017 Apr 27];12:380–424. Available from:
45
46
928 https://www.cambridge.org/core/product/identifier/S0001867800050230/type/journal_article
47
48

929 19. Bookstein FL. Biometrics, biomathematics and the morphometric synthesis. Bulletin of mathematical
49
50
930 biology [Internet]. 1996 [cited 2017 Apr 27];58:313–65. Available from:
51
52
931 <http://www.ncbi.nlm.nih.gov/pubmed/8713662>
53
54

932 20. James Rohlf F, Marcus LF. A revolution morphometrics. Trends in Ecology & Evolution [Internet]. 1993
55
56
933 [cited 2017 Apr 27];8:129–32. Available from:
57
58
934 <http://linkinghub.elsevier.com/retrieve/pii/016953479390024J>
59
60

935 21. Adams DC, Rohlf FJ, Slice DE. Geometric morphometrics: Ten years of progress following the
61
62
63
64
65

- 936 “revolution.” *Italian Journal of Zoology*. 2004;71:5–16.
2
- 937 22. Cardini A, Loy A. On growth and form in the “computer era”: from geometric to biological
938 morphometrics. In: Cardini A, Loy A, editors. *Virtual Morphology and Evolutionary Morphometrics in the*
939 *new millennium*. Associazione Teriologica Italiana; 2013. p. 1–5.
8
- 940 23. Cope J, Corney D, Clark J, Remagnino P, Wilkin P. Plant species identification using digital
941 morphometrics: a review. 2012; Available from: <http://dx.doi.org/10.1016/j.eswa.2012.01.073>
942
943
- 944 24. Claude J. Log-shape ratios, Procrustes superimposition, elliptic Fourier analysis: three worked examples
945 in R. In: Cardini A, Loy A, editors. *Virtual Morphology and Evolutionary Morphometrics in the new*
946 *millennium*. Associazione Teriologica Italiana; 2013. p. 94–102.
947
948
- 949 25. Zelditch ML, Sheets HD, Fink WL. Spatiotemporal Reorganization of Growth Rates in the Evolution of
950 Ontogeny. *Evolution* [Internet]. 2000;54:1363–71. Available from: <http://doi.wiley.com/10.1111/j.0014-3820.2000.tb00568.x>
951
952
- 953 26. MacLeod N, Krieger J, Jones KE. Geometric Morphometric Approaches to Acoustic Signal Analysis in
954 Mammalian Biology. In: Cardini A, Loy A, editors. *Virtual Morphology and Evolutionary Morphometrics in*
955 *the new millennium*. Associazione Teriologica Italiana; 2013. p. 110–25.
956
957
- 958 27. Cardini, Rohlf, Klingenberg, Adams et al. *Virtual Morphology and Evolutionary Morphometrics in the*
959 *new millenium* [Internet]. Cardini A, Loy A, editors. *Hystrix. The Italian Journal of Mammalogy*.
960 Associazione Teriologica Italiana; 2013. Available from:
961 [http://biocenosi.dipbsf.uninsubria.it/atit/PDF/Volumesupp\(2005\)/testo_estratti.pdf](http://biocenosi.dipbsf.uninsubria.it/atit/PDF/Volumesupp(2005)/testo_estratti.pdf)
962
963
- 964 28. Chitwood DH, Rundell SM, Li DY, Woodford QL, Yu TT, Lopez JR, et al. Climate and developmental
965 plasticity: interannual variability in grapevine leaf morphology. *Plant Physiology* [Internet].
966 2016;170:pp.01825.2015. Available from: <http://www.plantphysiol.org/content/170/3/1480.abstract?etoc>
967
968
- 969 29. Viscosi V. Geometric morphometrics and leaf phenotypic plasticity: Assessing fluctuating asymmetry
970 and allometry in European white oaks (*Quercus*). *Botanical Journal of the Linnean Society*. 2015;179:335–
971 48.
972
973
- 974 30. Viscosi V, Cardini A. Leaf morphology, taxonomy and geometric morphometrics: A simplified protocol
975 for beginners. *PLoS ONE*. 2011;6.
976
977
- 978 31. Scholthof KG, Adkins S, Czosnek H, Palukaitis P, Jacquot E, Hohn T, et al. Top 10 plant viruses in
979 molecular plant pathology. 2011;12:938–54.
980
981
- 982 32. Matthews REF (Richard EF, Hull R, Matthews REF (Richard EF. *Matthews’ plant virology*. [Internet].
983 Academic Press; 2002 [cited 2017 Aug 14]. Available from:
984
985

967 <http://www.sciencedirect.com/science/book/9780123611604>
2

968 33. Zavallo D, Debat HJ, Conti G, Manacorda CA, Rodriguez MC, Asurmendi S. Differential mRNA
3
4
5
969 accumulation upon early *Arabidopsis thaliana* infection with ORMV and TMV-Cg is associated with distinct
6
7
970 endogenous small RNAs level. *PLoS ONE*. 2015;10.
8

971 34. Manacorda CA, Mansilla C, Debat HJ, Zavallo D, Sánchez F, Ponz F, et al. Salicylic Acid Determines
9
10
972 Differential Senescence Produced by Two Turnip mosaic virus Strains Involving Reactive Oxygen Species
11
12
973 and Early Transcriptomic Changes. *Molecular plant-microbe interactions : MPMI* [Internet]. 2013;26:1486–
13
14
974 98. Available from: <http://www.ncbi.nlm.nih.gov/pubmed/23945002>
15
16

975 35. Sánchez F, Manrique P, Mansilla C, Lunello P, Wang X, Rodrigo G, et al. Viral Strain-Specific
17
18
976 Differential Alterations in *Arabidopsis* Developmental Patterns. *Molecular Plant-Microbe Interactions*.
19
20
977 2015;28:1304–15.
21
22

978 36. Doumayrou J, Leblaye S, Froissart R, Michalakakis Y. Reduction of leaf area and symptom severity as
23
24
979 proxies of disease-induced plant mortality: the example of the Cauliflower mosaic virus infecting two
25
26
980 Brassicaceae hosts. *Virus research* [Internet]. Elsevier B.V.; 2013 [cited 2014 Mar 21];176:91–100.
27
28
981 Available from: <http://www.ncbi.nlm.nih.gov/pubmed/23742852>
29
30

982 37. Ferrier T, Matus JT, Jin J, Riechmann JL. *Arabidopsis* paves the way: genomic and network analyses in
31
32
983 crops. *Current Opinion in Biotechnology* [Internet]. 2011 [cited 2017 Apr 27];22:260–70. Available from:
33
34
984 <http://www.sciencedirect.com/science/article/pii/S0958166910002284>
35

985 38. Aguilar I, Sánchez F, Martin AM, Martinez-herrera D, Ponz F. Nucleotide sequence of Chinese rape
36
37
986 mosaic virus (oilseed rape mosaic virus), a crucifer tobamovirus infectious on *Arabidopsis thaliana*. *Plant*
38
39
987 *molecular biology*. 1996;191–7.
40
41

988 39. Sánchez F, Martínez-Herrera D, Aguilar I, Ponz F. Infectivity of turnip mosaic potyvirus cDNA clones
42
43
989 and transcripts on the systemic host *Arabidopsis thaliana* and local lesion hosts. *Virus research* [Internet].
44
45
990 1998;55:207–19. Available from: <http://www.ncbi.nlm.nih.gov/pubmed/9725673>
46
47

991 40. Boyes DC, Zayed a M, Ascenzi R, McCaskill a J, Hoffman NE, Davis KR, et al. Growth stage-based
48
49
992 phenotypic analysis of *Arabidopsis*: a model for high throughput functional genomics in plants. *The Plant*
50
51
993 *cell* [Internet]. 2001;13:1499–510. Available from:
52
53
994 <http://www.pubmedcentral.nih.gov/articlerender.fcgi?artid=139543&tool=pmcentrez&rendertype=abstract>
54
55

995 41. Schutz H, Krieger J. *Guide to geometric morphometrics*. 2007.
56
57

996 42. Rohlf FJ. The tps series of software. *Hystrix, the Italian Journal of Mammalogy*. 2015;26:1–4.
58
59

997 43. Rohlf FJ. *Tps Series* [Internet]. New York: Department of Ecology and Evolution, State University of
60
61
62
63
64
65

998 New York, Stony Brook; 2017. Available from: <http://life.bio.sunysb.edu/morph/>
2

999 44. Zelditch ML, Swiderski DL, Sheets HD. Geometric morphometrics for biologists: a primer. London:
4 Academic Press; 2012.

1000
6

1001 45. Bookstein FL. Morphometric tools for landmark data: Geometry and biology. Cambridge: Cambridge
8 University Press; 1991.

1002
10

1003 46. Klingenberg CP. MorphoJ: An integrated software package for geometric morphometrics. *Molecular
12 Ecology Resources*. 2011;11:353–7.

1004
14

1005 47. Hammer Ø, Harper DAT, Ryan PD. PAST: Paleontological Statistics Software Package for Education
16 and Data Analysis. *Palaeontologia Electronica* [Internet]. 2001;4. Available from:
18
20 <http://folk.uio.no/ohammer/past>

1007
21

1008 48. Adams DC, Collyer ML. A general framework for the analysis of phenotypic trajectories in evolutionary
23 studies. *Evolution*. 2009;63:1143–54.

1009
24

1010 49. RStudio Team. RStudio: Integrated Development for R. [Internet]. Boston, MA: RStudio, Inc.; 2016.
26 Available from: <http://www.rstudio.com/>

1011
28

1012 50. Di Rienzo JA, Casanoves F, Balzarini MG, González L, Tablada M, Robledo CW. InfoStat versión 2012.
30 InfoStat Group, Facultad de Ciencias Agropecuarias, Universidad Nacional de Córdoba, Argentina.
32 [Internet]. 2012. Available from: <http://www.infostat.com.ar>

1013
34

1014 51. Gaetano J. Holm-Bonferroni Sequential Correction: An EXCEL Calculator. 2013.

1015
37

1016 52. Holm S. A Simple Sequentially Rejective Multiple Test Procedure. *Scand J Statist* [Internet]. 1979 [cited
39 2017 May 25];6:65–70. Available from: <http://www.jstor.org/stable/4615733>

1017
41

1018 53. Zaiontz C. Real Statistics Resource Pack software [Internet]. 2017. Available from: [www.real-](http://www.real-statistics.com)
43 [statistics.com](http://www.real-statistics.com)

1019
45

1020 54. Carreira VP, Soto IM, Mensch J, Fanara JJ. Genetic basis of wing morphogenesis in *Drosophila*: sexual
47 dimorphism and non-allometric effects of shape variation. *BMC developmental biology* [Internet]. *BioMed*
49 *Central*; 2011 [cited 2017 May 6];11:32. Available from: <http://www.ncbi.nlm.nih.gov/pubmed/21635778>

1021
51

1022 55. Rohlf FJ, Slice D. Extensions of the Procrustes Method for the Optimal Superimposition of Landmarks.
53 *Systematic Zoology* [Internet]. 1990 [cited 2017 May 9];39:40. Available from:
55 <https://academic.oup.com/sysbio/article-lookup/doi/10.2307/2992207>

1023
57

1024 56. Peaucelle A, Morin H, Traas J, Laufs P. Plants expressing a miR164-resistant CUC2 gene reveal the
59 importance of post-meristematic maintenance of phyllotaxy in *Arabidopsis*. *Development* (Cambridge,
61
62
63
64
65

1028 England) [Internet]. 2007;134:1045–50. Available from: <http://www.ncbi.nlm.nih.gov/pubmed/17251269>
2

1029 57. Bookstein FL. Advances in Morphometrics. In: Marcus LF, Corti M, Loy A, Naylor GJ, Slice DE,
3
4 editors. Advances in Morphometrics. New York: Plenum Press; 1996. p. 131–151.
5

1030 58. Dewulf A, De Meulemeester T, Dehon M, Engel M, Michez D. A new interpretation of the bee fossil
6
7 Melitta willardi Cockerell (Hymenoptera, Melittidae) based on geometric morphometrics of the wing.
8
9 ZooKeys [Internet]. Pensoft Publishers; 2014 [cited 2017 May 10];389:35–48. Available from:
10
11 <http://zookeys.pensoft.net/articles.php?id=3536>
12
13
14

1035 59. Bai M, McCullough E, Song K-Q, Liu W-G, Yang X-K. Evolutionary Constraints in Hind Wing Shape in
15
16 Chinese Dung Beetles (Coleoptera: Scarabaeinae). Sereno PC, editor. PLoS ONE [Internet]. Elsevier
17
18 Academic Press; 2011 [cited 2017 May 10];6:e21600. Available from:
19
20 <http://dx.plos.org/10.1371/journal.pone.0021600>
21
22

1039 60. Parés-Casanova PM, Allés C. No functional sexual dimorphism in Minorcan horse assessed by geometric
23
24 morphometric methods. Animal Genetic Resources/Ressources génétiques animales/Recursos genéticos
25
26 animales [Internet]. 2015 [cited 2017 May 10];56:91–5. Available from:
27
28 http://www.journals.cambridge.org/abstract_S2078633614000514
29
30

1043 61. Klingenberg CP. Visualizations in geometric morphometrics: How to read and how to make graphs
31
32 showing shape changes. Hystrix. 2013;24:15–24.
33

1045 62. Klingenberg CP. Size, shape and form: concepts of allometry in geometric morphometrics. Development
34
35 Genes and Evolution [Internet]. Development Genes and Evolution; 2016;1–25. Available from:
36
37 <http://dx.doi.org/10.1007/s00427-016-0539-2>
38
39

1048 63. Ciampaglio CN, Kemp M, McShea DW. Detecting changes in morphospace occupation patterns in the
40
41 fossil record: characterization and analysis of measures of disparity. Paleobiology [Internet]. 2001;27:695–
42
43 715. Available from: [http://www.bioone.org/doi/abs/10.1666/0094-
44
45 8373%282001%29027%3C0695%3ADCIMOP%3E2.0.CO%3B2](http://www.bioone.org/doi/abs/10.1666/0094-8373%282001%29027%3C0695%3ADCIMOP%3E2.0.CO%3B2)
46
47

1052 64. Sidlauskas B. Continuous and arrested morphological diversification in sister clades of characiform
48
49 fishes: A phylomorphospace approach. Evolution. 2008;62:3135–56.
50
51

1053 65. Gould SJ. Ontogeny and phylogeny. Cambridge, MA: Harvard University Press; 1977.
52
53

1055 66. Hingst-Zaher E, Marcus LF, Cerqueira R. APPLICATION OF GEOMETRIC MORPHOMETRICS TO
54
55 THE STUDY OF POSTNATAL SIZE AND SHAPE CHANGES IN THE SKULL OF *Calomys expdsus* .
56
57 Hystrix, the Italian Journal of Mammalogy. 2000;11:99–113.
58
59

1058 67. Zelditch ML, Lundrigan BL, Sheets HD, Garland T. Do precocial mammals develop at a faster rate? A
60
61

1059 comparison of rates of skull development in *Sigmodon fulviventer* and *Mus musculus domesticus*. *Journal of*
 2
 1060 *Evolutionary Biology*. 2003;16:708–20.
 4

1061 68. Verbeke G, Fieuws S, Molenberghs G, Davidian M. The analysis of multivariate longitudinal data: a
 6
 1062 review. *Statistical methods in medical research* [Internet]. NIH Public Access; 2014 [cited 2017 May
 8
 1063 19];23:42–59. Available from: <http://www.ncbi.nlm.nih.gov/pubmed/22523185>
 10

1064 69. Taiz L, Zeiger E. *Plant physiology*. 4th ed. Sinauer Associates Inc., editor. Sunderland; 2006.
 12

1065 70. Pigliucci M. Studying the plasticity of phenotypic integration in a model organism. In: Pigliucci M,
 13
 1066 Preston K, editors. *Phenotypic integration: studying the ecology and evolution of complex phenotypes*. New
 16
 1067 York: Oxford University Press on Demand; 2004. p. 155–75.
 18

1068 71. Punyasena SW, Smith SY. *Bioinformatic and Biometric Methods in Plant Morphology*. Applications in
 20
 1069 *Plant Sciences* [Internet]. 2014;2:1400071. Available from:
 22
 1070 <http://www.bioone.org/doi/abs/10.3732/apps.1400071>
 24

1071 72. Apelt F, Breuer D, Nikoloski Z, Stitt M, Kragler F. Phytotyping ^{4D}: a light-field imaging system for non-
 26
 1072 invasive and accurate monitoring of spatio-temporal plant growth. *The Plant Journal* [Internet]. 2015 [cited
 28
 1073 2017 Jun 7];82:693–706. Available from: <http://www.ncbi.nlm.nih.gov/pubmed/25801304>
 30

1074 73. Gómez JM, Torices R, Lorite J, Klingenberg CP, Perfectti F. The role of pollinators in the evolution of
 32
 1075 corolla shape variation, disparity and integration in a highly diversified plant family with a conserved floral
 34
 1076 bauplan. *Annals of Botany* [Internet]. 2016 [cited 2017 May 23];117:889–904. Available from:
 36
 1077 <http://www.ncbi.nlm.nih.gov/pubmed/26884512>
 38
 1078
 40
 1079
 42
 43
 44
 45
 46
 47
 48
 49
 50
 51
 52
 53
 54
 55
 56
 57
 58
 59
 60
 61
 62
 63
 64
 65

1080 Table 1

Discriminant Function Analysis	3 DPI	4 DPI	5 DPI	6 DPI	7 DPI	8 DPI	10 DPI	12 DPI
Difference between means:								
Procrustes distance:	0.037	0.047	0.063	0.087	0.097	0.105	0.149	0.189
Mahalanobis distance:	1.799	1.924	3.815	5.117	6.651	7.035	9.078	10.863
T-square:	31.637	36.170	142.264	255.916	432.438	483.790	805.573	1153.389
<i>P-value (parametric):</i>	0.521	0.405	0.001	<0.0001	<0.0001	<0.0001	<0.0001	<0.0001
P-values for permutation tests (1000 permutation runs):								
<i>Procrustes distance:</i>	0.549	0.182	0.005	0.002	<0.0001	<0.0001	<0.0001	<0.0001
<i>T-square (Mahalanobis distance):</i>	0.523	0.417	0.001	<0.0001	<0.0001	<0.0001	<0.0001	<0.0001

1081
23
1082
25
26
27
28
29
30
31
32
33
34
35
36
37
38
39
40
41
42
43
44
45
46
47
48
49
50
51
52
53
54
55
56
57
58
59
60
61
62
63
64
65

1083

Table 2

ORMV3-12 DPI		
		<i>p-value</i>
$MD_{Mock,ORMV}$	0.100	0.003
$\theta_{Mock,ORMV}$	18,34°	0.001
$D_{ShapeMock,ORMV}$	0.367	0.001
MPL_{Mock}	0.696	2.50E-04
MPL_{ORMV}	0.596	
$\sum Var_{Mock}$	0.035	2.52E-06
$\sum Var_{ORMV}$	0.023	
$D_{1(Mock)}$	20.21	2.89E-06
$D_{1(ORMV)}$	26.93	
Hyperellipse _{(IC95%)Mock}	0.022	0,005 *
Hyperellipse _{(IC95%)ORMV}	0.014	
$D_{2(Mock)}$	32.97	0,040 *
$D_{2(ORMV)}$	41.87	
ORMV4-10 DPI		
$MD_{Mock,ORMV}$	0.085	0.005
$\theta_{Mock,ORMV}$	16,46°	0.001
$D_{ShapeMock,ORMV}$	0.343	0.037
MPL_{Mock}	0.472	8,03E-04 *
MPL_{ORMV}	0.401	
$\sum Var_{Mock}$	0.022	2,21E-05 *
$\sum Var_{ORMV}$	0.015	
$D_{1(Mock)}$	21.77	3,61E-05 *
$D_{1(ORMV)}$	28.37	
Hyperellipse _{(IC95%)Mock}	0.012	0,075 *
Hyperellipse _{(IC95%)ORMV}	0.009	
$D_{2(Mock)}$	48.94	0,203 *
$D_{2(ORMV)}$	56.41	
TuMV4-10 DPI 1st		
$MD_{Mock,TuMV}$	0.093	0.015
$\theta_{Mock,TuMV}$	34,41°	0.001
$D_{ShapeMock,TuMV}$	0.613	0.001
MPL_{Mock}	0.504	0,049 *
MPL_{TuMV}	0.461	
$\sum Var_{Mock}$	0.030	0,007 *
$\sum Var_{TuMV}$	0.023	
$D_{1(Mock)}$	16.94	0,017 *
$D_{1(TuMV)}$	21.83	
Hyperellipse _{(IC95%)Mock}	0.019	0,156 *
Hyperellipse _{(IC95%)TuMV}	0.017	
$D_{2(Mock)}$	32.51	0,277 *
$D_{2(TuMV)}$	46.05	
TuMV4-10 DPI 2nd		
$MD_{Mock,TuMV}$	0.082	0.202
$\theta_{Mock,TuMV}$	35,05°	0.001
$D_{ShapeMock,TuMV}$	0.642	0.002

*= First 3 PCs considered (>95% total variance)

Units: MD = DShape = MPL = D1 = D2 = Euclidean distance.

θ = degrees. $\sum Var$ = Hyperellipse(CI=95%) = dimensionless.

Statistically significant results in bold

1084

1085

1086

1087

1088

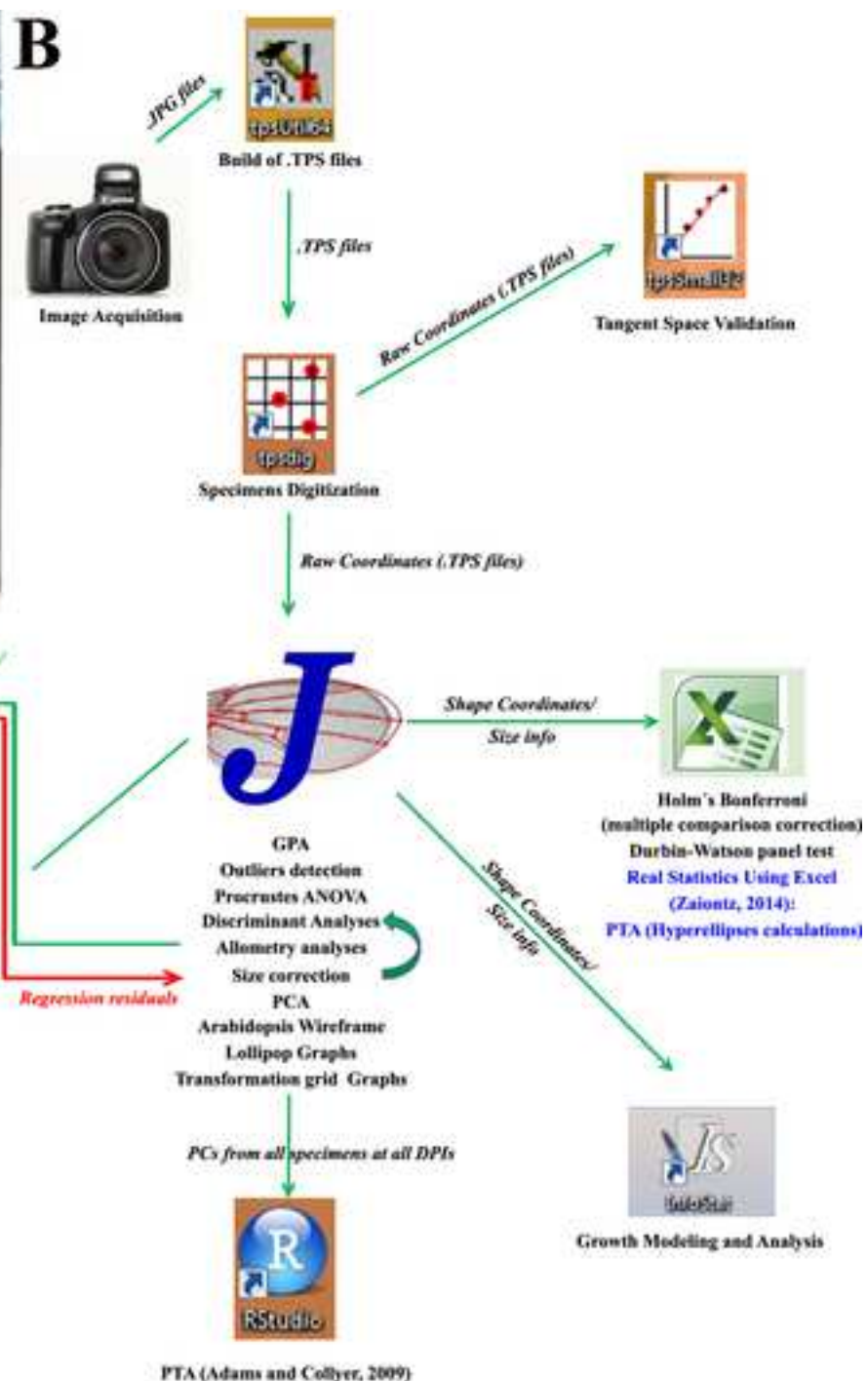
61

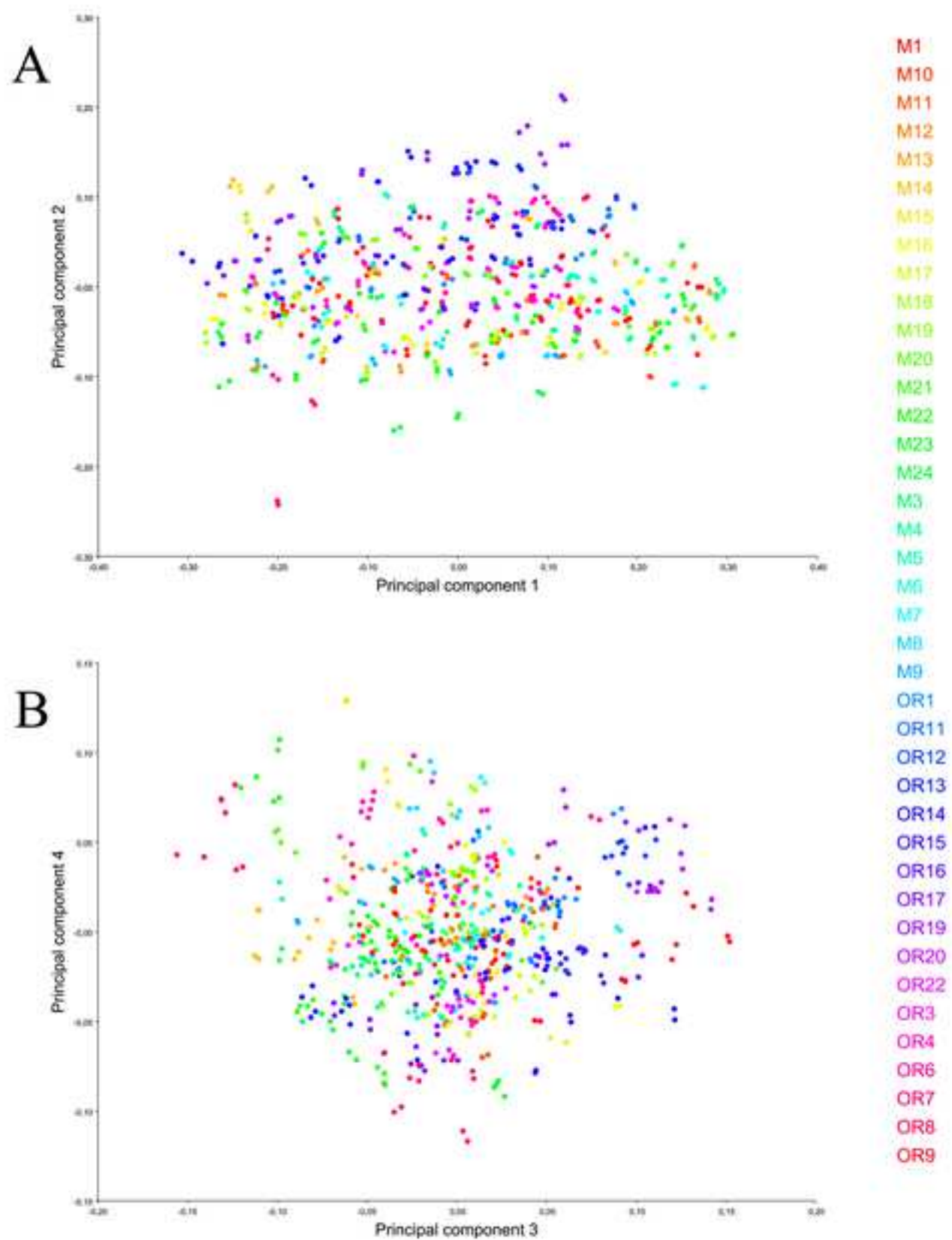
62

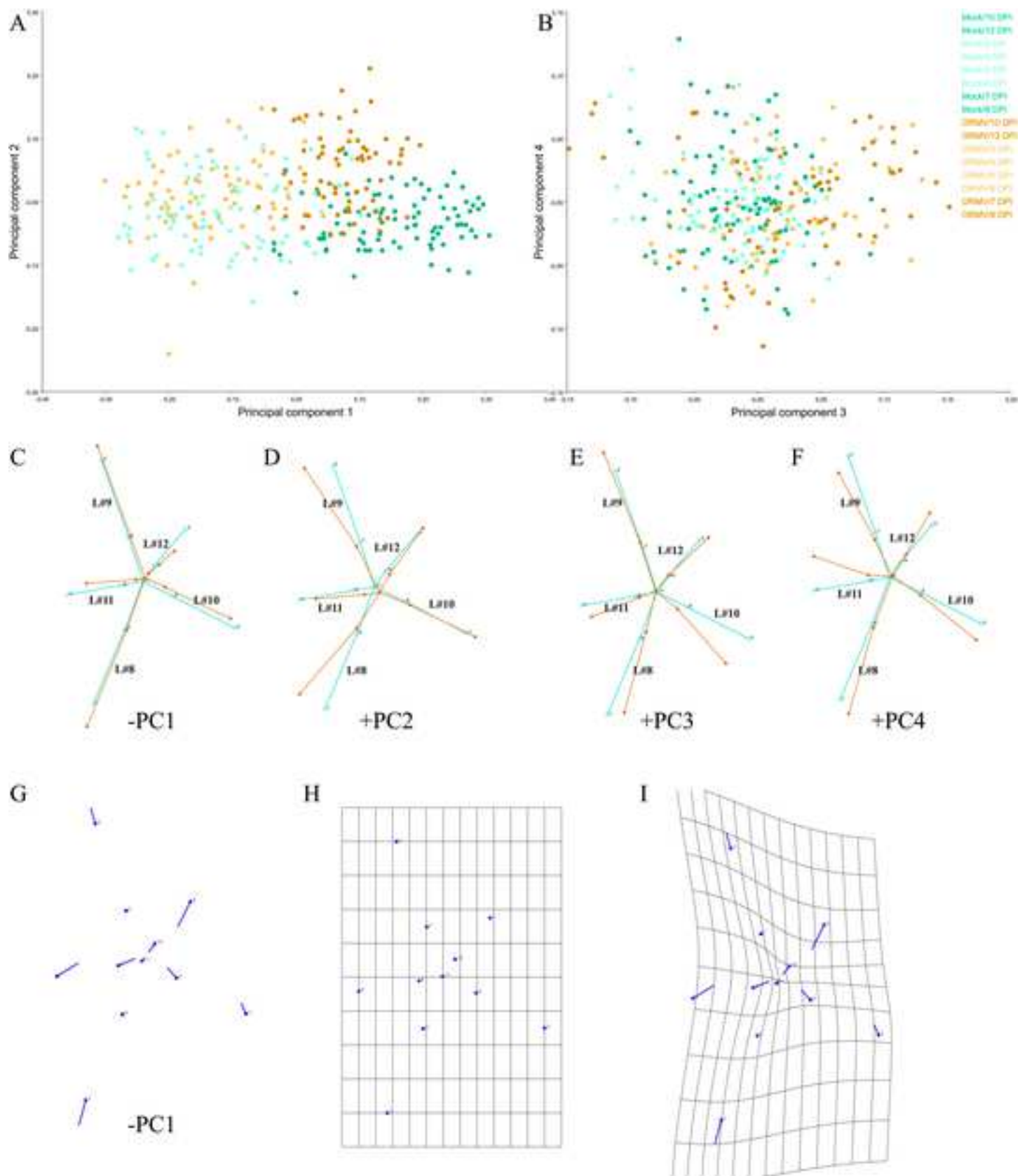
63

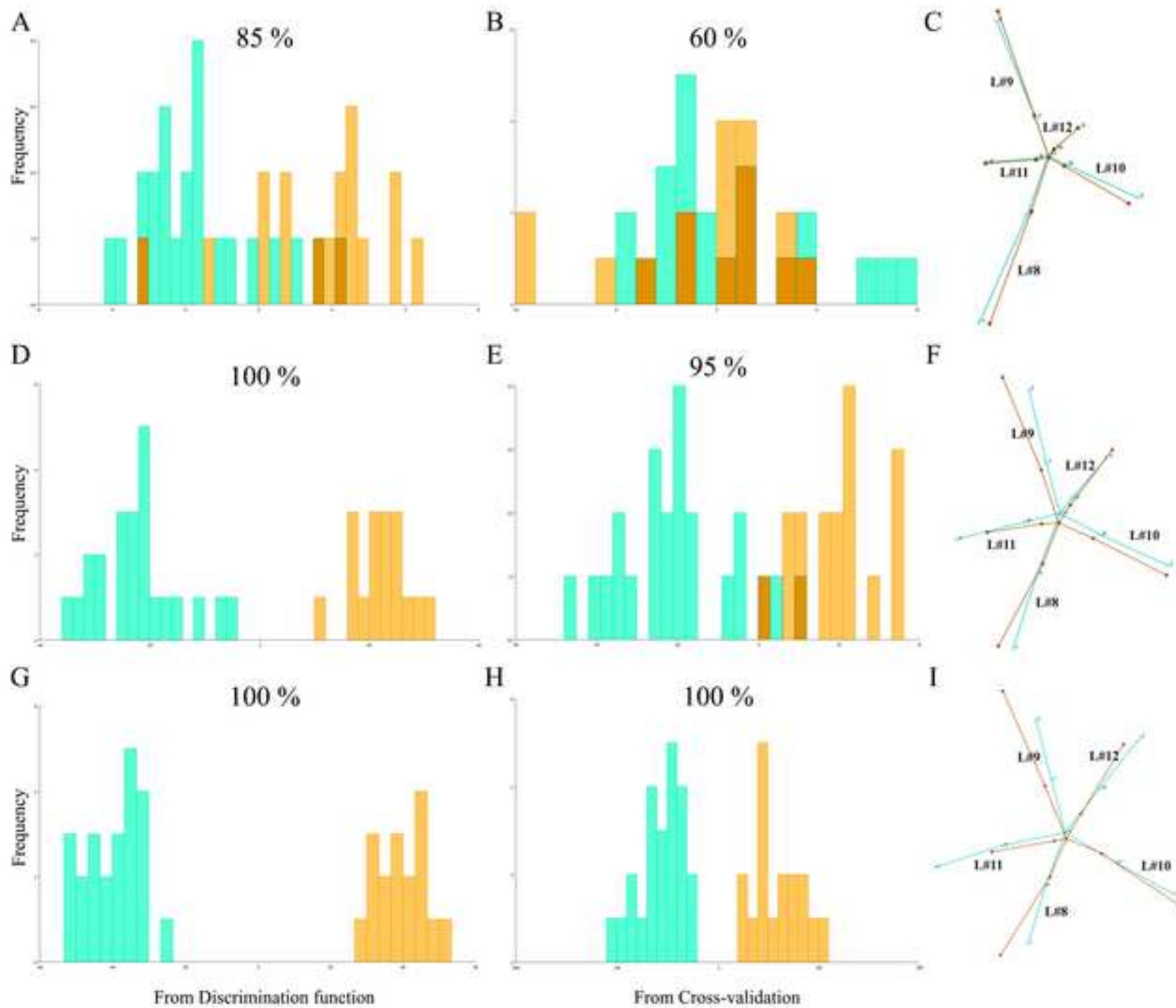
64

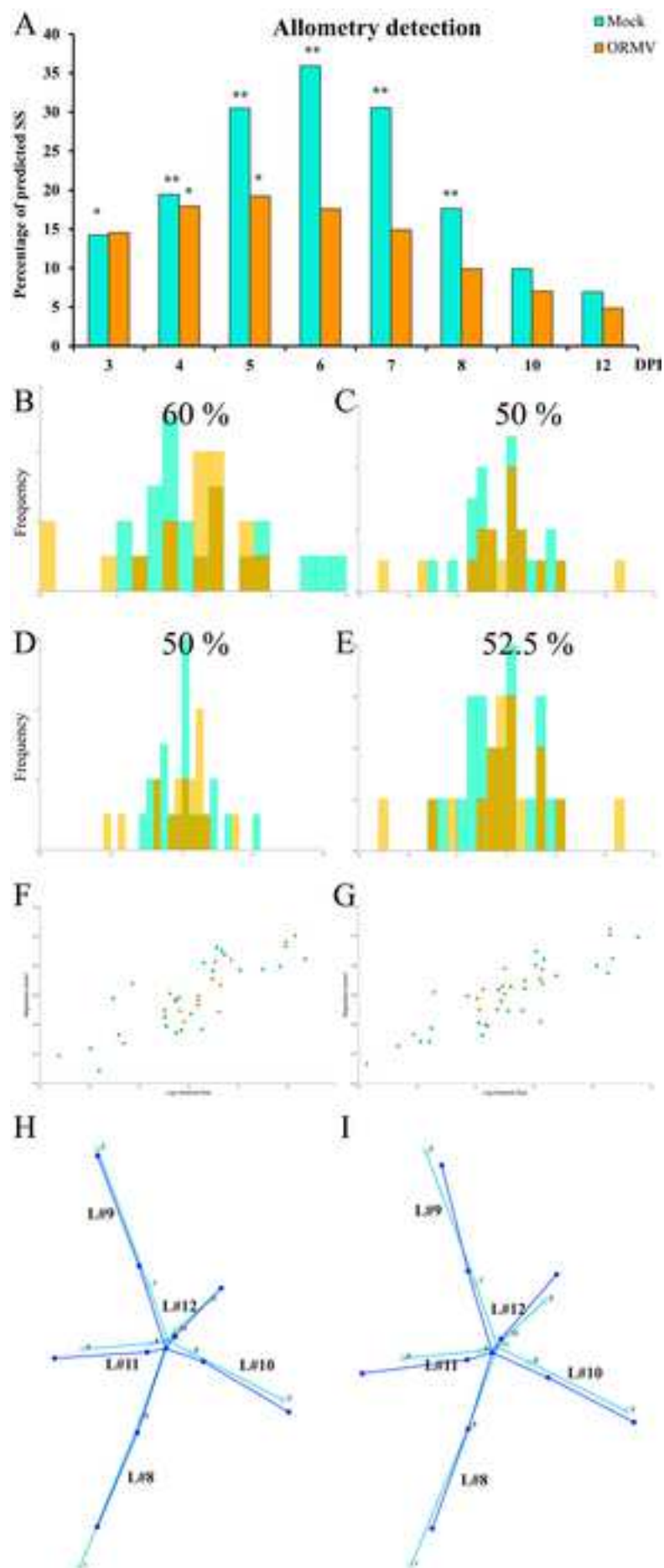
65

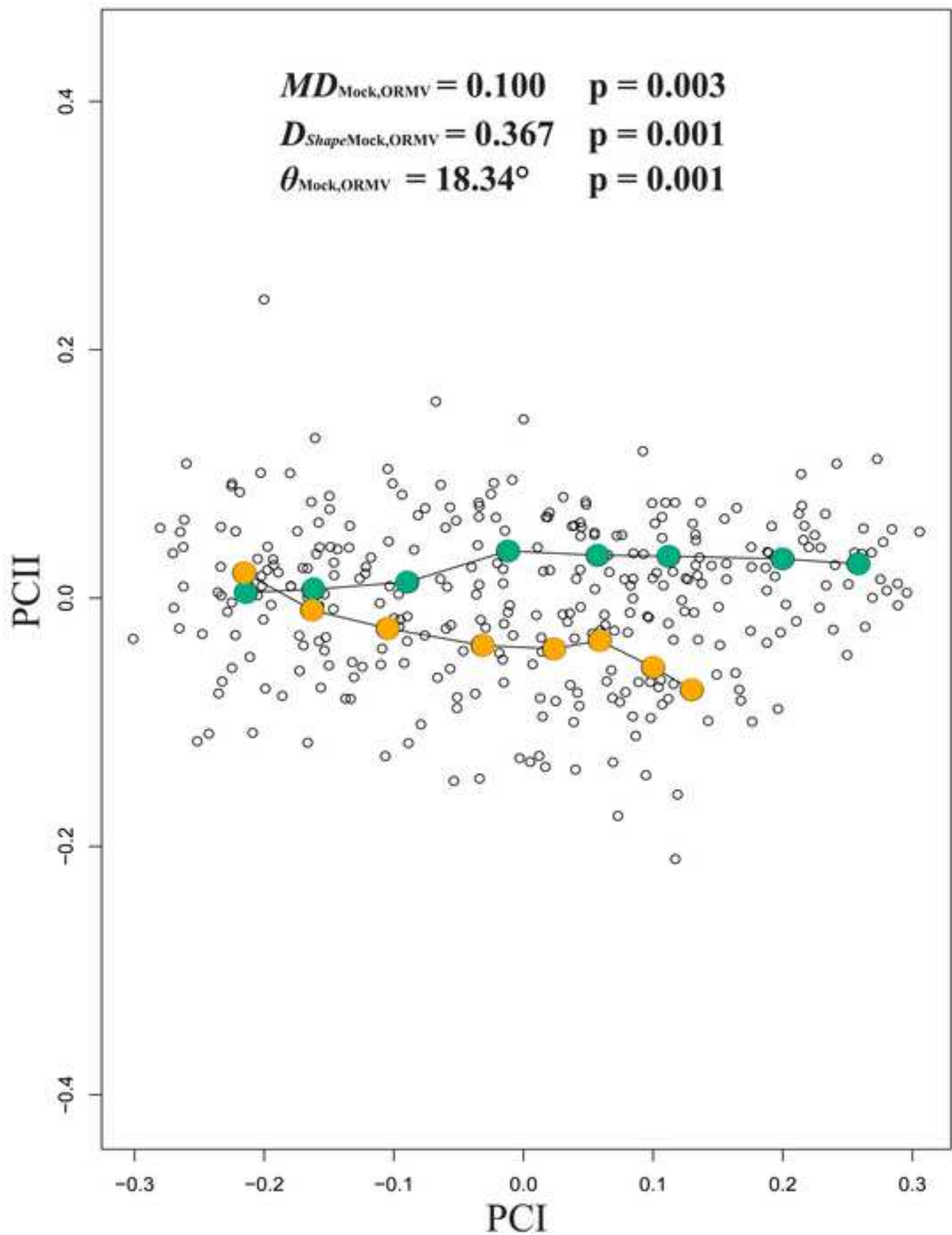


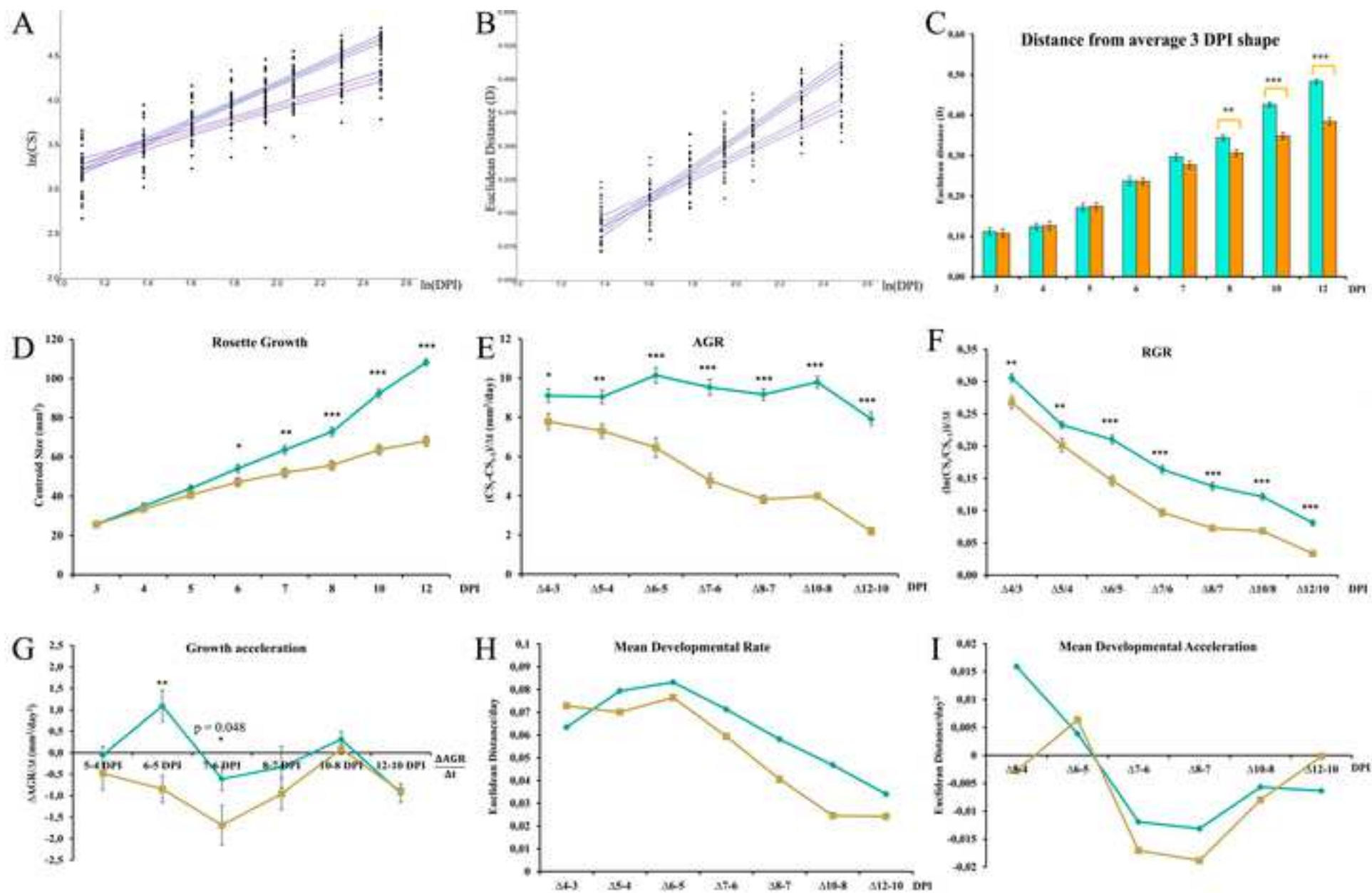


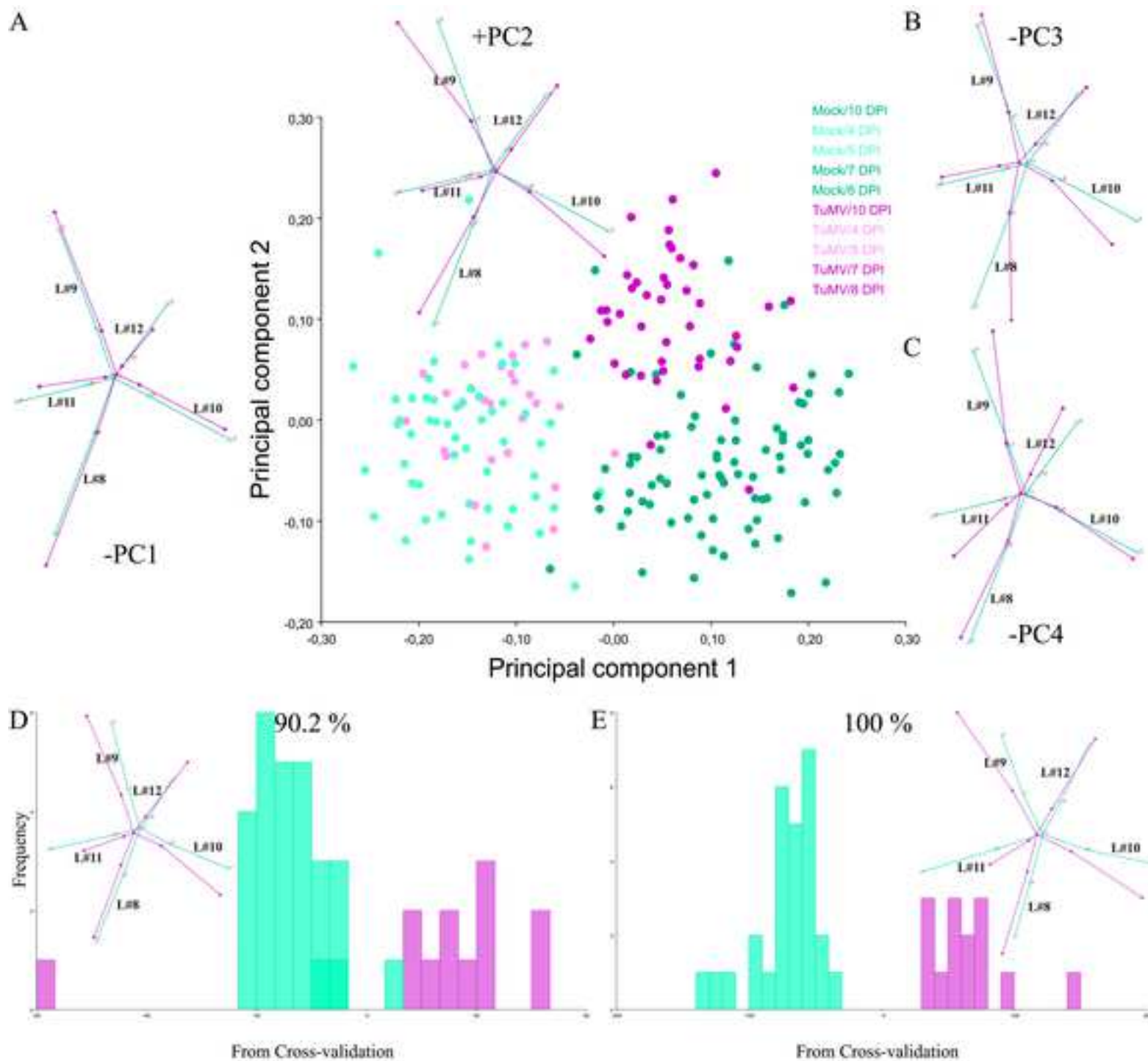


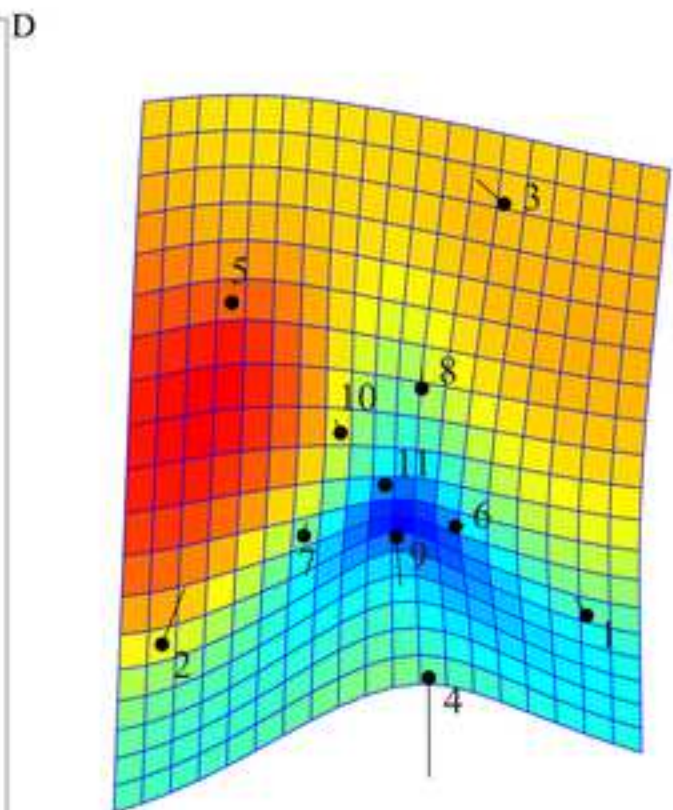
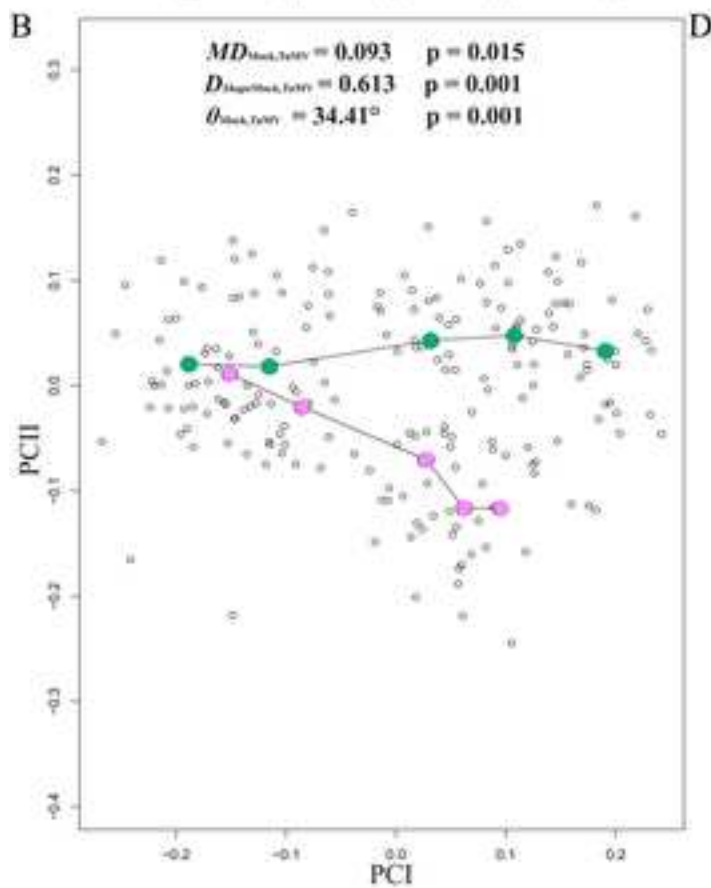
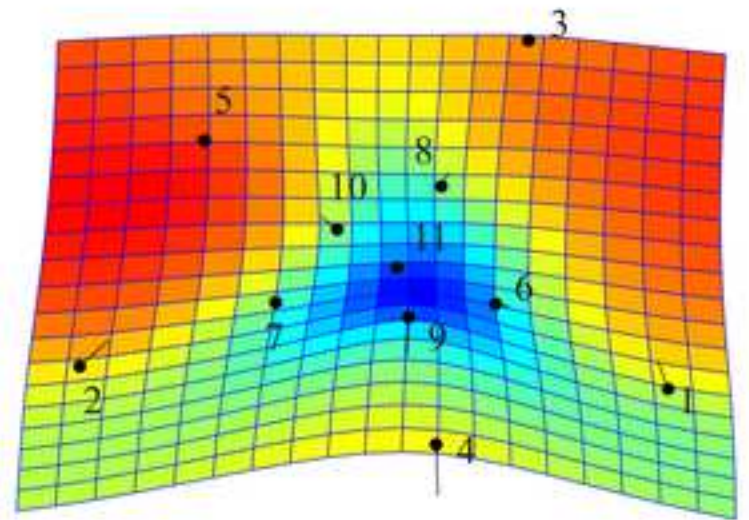
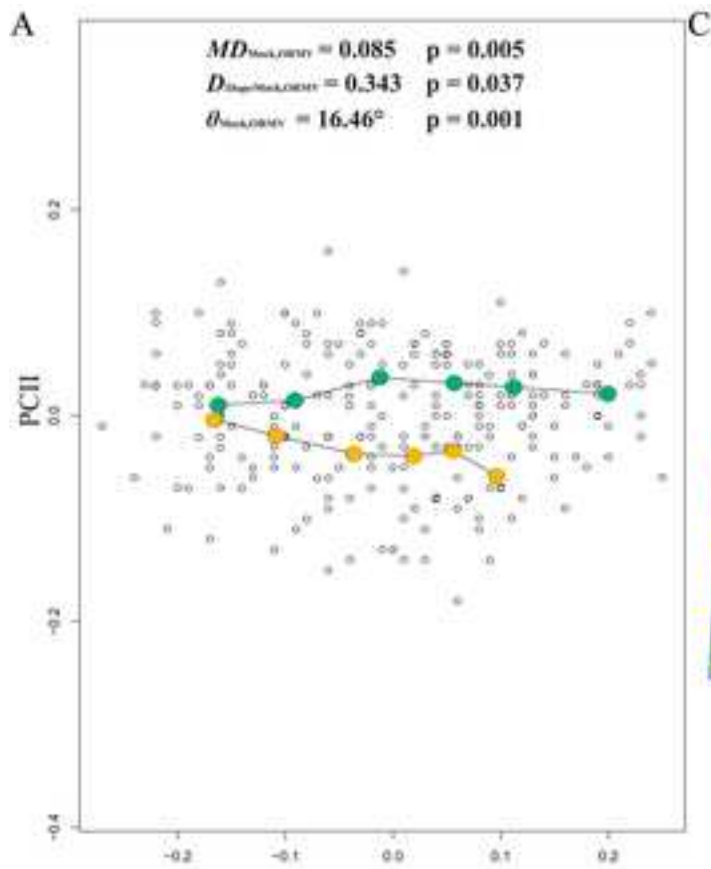










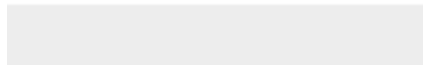








Click here to access/download
Supplementary Material
Supplementary Table 1.xlsx



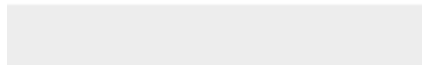


Click here to access/download
Supplementary Material
Supplementary Table 2.xlsx



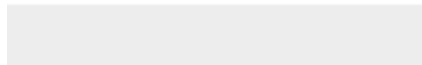


Click here to access/download
Supplementary Material
Supplementary Table 3.xlsx



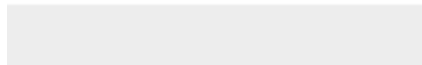


Click here to access/download
Supplementary Material
Supplementary Table 4.xlsx






Click here to access/download
Supplementary Material
Supplementary Table 5.xlsx





Click here to access/download
Supplementary Material
Supplementary file TuMV 1st





Click here to access/download
Supplementary Material
Supplementary file TuMV 2nd

